

High-Throughput Mapping of a Dynamic Signaling Network In Mammalian Cells

Miriam Barrios-Rodiles¹, Kevin R. Brown², Barish Ozdamar^{1,3}, Zhong Liu¹, Robert S. Donovan¹, Fukiko Shinjo¹, Yongmei Liu¹, Rohit Bose^{1,3}, Joanna Dembowy^{1,3}, Ian W. Taylor^{1,3}, Valbona Luga^{1,3}, Natasa Przulj⁴, Mark Robinson⁵, Harukazu Suzuki⁶, Yoshihide Hayashizaki⁶, Igor Jurisica^{2,4,7} and Jeffrey L. Wrana^{1,3}

¹ Program in Molecular Biology and Cancer
Samuel Lunenfeld Research Institute
Mount Sinai Hospital, Toronto M5G 1X5, Canada

² Department of Medical Biophysics
University of Toronto, Toronto M5G 2M9, Canada

³ Department of Medical Genetics and Microbiology
University of Toronto, Toronto M5S 1A8, Canada

⁴ Department of Computer Science
University of Toronto, Toronto, Ontario, Canada M5S 3H5

⁵ Banting and Best Department of Medical Research
University of Toronto, Toronto, Ontario, M5G 1L6, Canada

⁶ Laboratory for Genome Exploration Research Group
RIKEN Genomic Sciences Center (GSC) Yokohama Institute
1-7-22 Suehiro-cho, Tsurumi-ku, Yokohama, 230-0045, Japan

⁷ Division of Cancer Informatics
Ontario Cancer Institute
Princess Margaret Hospital, Toronto M5G 2M9

Correspondence to:
Dr. Jeffrey L. Wrana
Senior Scientist
Rm 1075, SLRI
Mount Sinai Hospital
600 University Ave.
Toronto ON, Canada M5G 1X5
Tel: (416)586-4800(x2791)
Fax: (416)586-8869

Email: wrana@mshri.on.ca

ABSTRACT

Signaling pathways transmit information through protein interaction networks that are dynamically regulated by complex extracellular cues. We developed an automated high-throughput technology we call LUMIER to analyze dynamic protein-protein interaction networks in mammalian cells. LUMIER was used to systematically analyze the interaction of 518 proteins with components of the TGF β pathway and identified 901 interactions from 11,914 tests. Analysis of the Smad network module in the presence and absence of TGF β signaling revealed a dynamic network in which numerous interactions were lost, while others were gained. The TGF β LUMIER network was analyzed using the BTSVQ algorithm, which incorporates self-organizing maps and k -means clustering. This identified a group of proteins that showed similar interactions with the TGF β pathway and included components of both the p21 activated kinase (PAK) and polarity pathways. Moreover, TGF β receptors made numerous connections with these two networks that otherwise display only sparse connectivity. High-throughput mapping of protein interactions in mammalian cells thus demonstrates a link between the TGF β pathway and both the PAK and polarity subnetworks, that yields a large interconnected network involved in cell motility and polarity.

Dynamic protein-protein interactions (PPIs) are key for cell signaling and dictate timing and intensity of network outputs. However, systematic mapping of PPI networks have thus far focussed on static analyses in *S. cerevisiae*, *D. melanogaster* and *C. elegans* (1-6). Therefore, to begin building an understanding of how signaling networks convey information in vertebrates we developed a high-throughput (HTP) strategy to systematically map PPIs in mammalian cells. This strategy, which we call LUMIER, for LUminescence-based Mammalian IntERactome mapping (Fig. 1A), employs Renilla luciferase enzyme (RL) fused to proteins of interest. RL-tagged proteins are then co-expressed with individual Flag-tagged partners in mammalian cells and interaction determined by performing an RL enzymatic assay on anti-Flag immunoprecipitates.

Validation of LUMIER. As a model for a systematic study of mammalian cell signaling, we focussed on the TGF β superfamily of extracellular morphogens, which regulate a plethora of biological processes in metazoans (7-11). The superfamily includes the TGF β s, bone morphogenetic proteins (BMPs) and activins, which signal through heteromeric complexes of type II and type I transmembrane ser/thr kinase receptors. The receptor complex is activated when the type II receptor kinase transphosphorylates the type I receptor (Fig. 1B), which stimulates binding and phosphorylation of receptor-regulated Smads (R-Smads) by the type I receptor. R-Smad2 and R-Smad3 function in TGF β signaling, whereas the BMPs through different type I receptors (ALK2, ALK3 and ALK6) activate R-Smad1, R-Smad5 and R-Smad8. Phosphorylated R-Smads dissociate from the receptor, form a complex with the common mediator Smad, Smad4, and this

complex then accumulates in the nucleus where it regulates transcription by interacting with DNA binding proteins (12).

The Smad pathway provides an example of how post-translational modifications (PTMs) regulate the dynamics of PPI networks to control signal transduction (13, 14). Therefore, we used this pathway to determine whether LUMIER could map PTM-dependent interactions (Fig. 1). For this, we fused RL to Smad4 (Smad4-RL) and co-expressed it with Flag-Smad2 or the TGF β receptor phosphorylation site mutant, Flag-Smad2(2SA), which does not bind Smad4. In the absence of signaling, little if any Smad4-RL was found associated with Smad2 (Fig. 1C), whereas TGF β signaling induced strong association with WT Smad2 that was revealed by high levels of RL activity in the immune complexes (15). In contrast, no Smad4-RL was detected in Smad2(2SA) immunoprecipitates. We also examined signal-specific interactions using the BMP pathway and observed increased Smad4-RL bound to Flag-Smad1 but not Smad2, upon activation of BMP signaling (Fig. 1D). LUMIER also recapitulated constitutive interactions such as that between Smad4 and the co-repressor SnoN (Fig. 1E). Furthermore, it detected the transient interaction between Smad2 and constitutively active RL-tagged T β RI (Fig. 1F) that is difficult to detect by traditional means. Thus, LUMIER recapitulates pathway-specific PTM-dependent PPIs, constitutive protein interactions and interactions involving transmembrane receptors. The latter is noteworthy as transmembrane receptors are critical focal points in signaling networks, are important drug targets and have been difficult to study using HTP approaches (16).

High-throughput LUMIER. LUMIER demonstrated very high sensitivity and faithfully recapitulated dynamic interactions in the TGF β pathway, suggesting that it might be amenable for mapping PPI networks in mammalian cells. For proof of principle, we optimized LUMIER in a 96-well format and performed a pilot-screen of Smad4-RL against 30 different Flag-tagged cDNAs in the presence or absence of TGF β signaling (Fig. 2A). This revealed low background and strong, signal-dependent interactions between Smad4-RL and either Flag-Smad2 or Flag-Smad3, as well as the interaction of Smad4-RL with Flag-Ski, as previously reported (17). Therefore, LUMIER is amenable to HTP systematic mapping of PPIs in mammalian cells. To map a TGF β PPI network, we RL-tagged core members of the pathway that included type I receptors, Smads, and the Smad regulatory ubiquitin ligases, Smurf1 and Smurf2 (Table S1). To systematically evaluate PPIs we used the FANTOM1 library of mouse cDNAs (18) and 3Flag-tagged 518 cDNAs (Fig. S1) that contained at least one of the domains summarized in Fig. 2B (15). This panel contained both well-characterized proteins and proteins of unknown function. Each tagged protein was then transiently expressed in mammalian cells and expression confirmed by automated immunofluorescence microscopy using a Cellomics Arrayscan system, which also allowed characterization of their subcellular localization (Fig. S2).

To analyze the interaction of each RL-tagged TGF β pathway component in different signaling contexts with every Flag-tagged protein required approximately 12,000 experiments. Therefore, we used a robotics platform and performed automated LUMIER (15). To visualize the entire dataset, we generated a diagram in which each screen with RL-tagged protein is represented on the vertical axis and Flag-tagged proteins are on the

horizontal axis (Fig. 2B). The results of each PPI test are represented by a bar at the intersection, with tone of yellow reflecting the intensity, calculated as fold change over the negative control. We refer to this as the LUMIER interaction intensity ratio (LIR) (see Table S2 for all LIR values). This overview of LUMIER results revealed some global features of protein partners of TGF β pathway components. For example, we observed that ras GTPase or kinase domain-containing proteins displayed numerous interactions. In contrast, others, such as phospho-tyrosine-binding SH2 domains, displayed a paucity of interactions, consistent with our present understanding of TGF β signaling, which is dominated by ser/thr phosphorylation events. This suggests that the TGF β pathway preferentially interacts with certain classes of signaling molecules.

Analysis of the TGF β interactome. LUMIER not only provides qualitative information regarding PPIs, but also conveys quantitative data. The LIR can thus provide important information regarding the confidence in an interaction and its dynamic regulation by cell signaling pathways. Therefore, at low LIRs, background noise predominates, resulting in high false positive rates and a noisy network, whereas, at higher LIRs, interactions will be of high confidence, but many important interactions that may be transient, occur in specific compartments or are of lower affinity, will be undetected. Therefore, to build the interaction network graph, we examined false negative rates and, although difficult to accurately measure, false positive rates, as well as the statistical significance of interactions at different LIR cutoffs (15). Based on these analyses, we chose a conservative LIR cutoff of 3, which yielded false negative rates of about 30% and approximate false positive rates of 16%. Of note, important interactions may exist below this cutoff, and in the future the LUMIER 1.5 fold cutoff graph may be explored for

biologically relevant networks by computationally integrating diverse datasets such as gene expression and protein localization (Fig. S2) (19-21).

Analysis of the TGF β interaction network at a LIR cutoff of 3 revealed 901 interactions amongst 276 proteins. These interactions formed an interconnected network with nodes displaying degrees that ranged from 1 to 130. Analysis of the degree distribution and clustering of the network revealed features of a scale-free network with possible hierarchical modularity (15) (Fig. S3). These topological features have also been noted in other PPI networks as well as other biological and real world networks (5, 22-26).

The TGF β signaling network is dynamic. Analyses of network dynamics is important in understanding biological systems (27), particularly in the case of signaling networks such as the TGF β system, which must be remodeled both in time and space in order to convey information (Fig. 1B). To determine how signaling regulates PPIs in our network, we focused on the dynamics of the Smad2 and Smad4 interactome in the absence and presence of TGF β signaling (Fig. 3B) and Smad1 with BMP signaling (Table S2). To capture the dynamics we also generated a movie of the network changes (Movie S1). Analysis of these graphs and in particular the movie revealed considerable partner switching. Thus, numerous interactions were lost upon signaling, whereas others, such as the assembly of Smad complexes, were stimulated. This was particularly evident for Smad4, possibly reflecting modulation of its protein interaction surfaces upon assembly into complexes with phosphorylated R-Smads. We next surveyed the network, which included the known interactions amongst the R-Smads and Smad4, and the interaction of Smad4 with CAMK, which phosphorylates Smad4 (28). We also verified,

by immunoprecipitation and immunoblotting, a number of previously undescribed interactions (data not shown). In particular, Smad2 association with the homeodomain transcription factor goosecoid, the C2-WW-HECT ubiquitin ligase, WWP2, and the protein phosphatase 2 regulatory subunit, PPP2R2D, as well as interactions between Smad4 and either Map kinase kinase 3 (MAP2K3) or TC21 (RRAS2). The identification of WWP2, extends the range of C2-WW-HECT ubiquitin ligases that function in Smad signaling beyond the Smurf subfamily and the presence of PPP2R2D suggests one potential mechanism for turning off Smad signaling by dephosphorylation. Indeed, overexpressed PPP2R2D was found to inhibit TGF β -dependent Smad signaling (data not shown). The interaction of MAP2K3 with Smads is also intriguing, since Smad7 has previously been found to bind MAP2K3 and this kinase is required for TGF β -dependent activation of p38 (29). These studies thus identify considerable dynamics in the Smad network that are more complex than simple signal-dependent association with effector molecules. It will be interesting to understand what aspects of TGF β biology are controlled by these fluxes.

The TGF β receptor links the PAK1 and Polarity clusters. To identify novel TGF β signaling networks of particular biological importance, we explored the TGF β LUMIER dataset using a Binary Tree-Structured Vector Quantization (BTSVQ) algorithm, which combines tree-structured vector quantization and partitive k -means clustering (30). BTSVQ is useful for clustering high-dimensional datasets since it performs unsupervised clustering of both dimensions, and supports intuitive visualization of clusters, both as a binary tree dendrogram, and component planes of Kohonen's Self-Organizing Maps (SOMs). SOMs employ a neural network algorithm that clusters high dimensional data

within a two-dimensional component plane, placing similar data in the same area of the map. SOMs thus provide a powerful method to compress information content, visualize complex datasets and effectively exploit the quantitative information inherent in LUMIER. Therefore we clustered prey space (all the 3Flag-tagged cDNAs) using BSVQ and identified homogeneous clusters. One of these included p21 activated kinase-1 (PAK1). PAKs are a family of kinases involved in regulating cytoskeletal dynamics, cell motility, survival, proliferation and gene expression through a variety of effectors (31). PAK activity is regulated by the low molecular weight GTPases Cdc42 and Rac1, which are activated by PAK interacting exchange factors, α -PIX and β -PIX.

PAKs were noteworthy because they have previously been implicated in TGF β signaling (32, 33), although physical association with TGF β pathway components have not been reported. Therefore, we anchored our unsupervised clustering on PAK1 and sorted the component planes to identify similar profiles. This yielded a cluster with a SOM profile that was clearly distinct from others, such as that containing IRF3 (Fig. 4A). This cluster contained known components, such as PAK1, as well as poorly characterized proteins such as ser/thr kinase STK22D and a pseudo-kinase (FLJ23356) we call TRIK (for TGF β receptor interacting pseudo kinase). Remarkably, other component planes in this cluster included the PAK-interacting proteins, ARHGEF6 (α -PIX) and Oxidative Stress Response kinase-1 (OSR1) (31, 34). Therefore, we focussed on this cluster and examined binding to affinity-labeled receptor complexes. This showed a range of interactions from weak (Fbx034) to strong (PAK1) (Fig. 4B). Of note, both OSR1 and α -PIX bound to receptors (Fig. 4B), as did the related β -PIX, which interacted with both T β RII and receptor complexes (Fig. S4A). Cdc42 is a key player in PAK signaling and is

activated by TGF β (35). Therefore, we extended our analysis to Cdc42, which we showed interacted with cell surface receptor complexes (Fig. S4B). Further, we observed that endogenous receptors bound specifically to a GST-CRIB affinity resin, which binds active Cdc42 and Rac1 (Fig. S4C), suggesting the possibility that active Cdc42 and Rac may bind to TGF β receptors. Finally, we examined endogenous interactions using a mouse mammary gland epithelial cell line, and observed endogenous PAK1 bound to endogenous T β RI (Fig. 4C). Thus, we define a previously unknown link between TGF β receptors and the PAK network that might suggest a model in which TGF β receptors regulate PAK signaling by nucleating assembly of a Cdc42, PIX and PAK complex.

This cluster also contained one other notable member, Occludin, which we confirmed interacted with endogenous T β RI (Fig. 4D) and receptor complexes (Fig. 4E). Occludin is a tight junction (TJ) accessory phosphoprotein that has four transmembrane domains, three cytoplasmic domains and two extracellular loops. Occludin interacts with a number of proteins (Reviewed in (36)) including those that link it to the polarity network, which controls cell polarity and in epithelial cells regulates tight junction homeostasis and epithelial cell plasticity. The striking similarity in the SOMs of PAK1 components and Occludin thus prompted us to examine in the literature the physical relationship between these two networks. This revealed that they were only sparsely connected to each other (Fig. 4Fi). However, inclusion of the novel interactions with TGF β pathway components identified in this study generated significant interconnectivity between the networks. In particular, the TGF β receptor linked extensively to the PAK1 network, as well as the polarity complex through Par6 (Fig. 4Fii). Furthermore, we show in a separate study that the link to Par6 is critical for TGF β -dependent epithelial-to-mesenchymal transition (37).

These results highlight the power of merging supervised and unsupervised clustering using BTSVQ analysis to extract and identify important PPI networks from LUMIER data. Furthermore, they reveal previously unappreciated complexity in signaling pathways regulated by TGF β receptors and suggest that Ser/Thr kinase receptors form a hub that interconnects the PAK, polarity and Smad networks.

Defining how cell signaling PPI networks control mammalian cell function is one key goal of systems biology. Here we report the first systematic analysis in mammalian cells of protein interactions involved in cell signaling. Our approach allows for recapitulation of PTMs that are essential for controlling network flux during signaling. Although our strategy employs overexpressed proteins, analysis of assay performance suggests it is robust, a conclusion supported by our identification of many known, as well as readily validated novel interactions. Recently, a systematic analysis of the TGF β -family dauer pathway in *C. elegans* employed Y2H coupled to genetic analysis (38). This identified a number of genes involved in the pathway, including *daf-5*, a *C. elegans* homolog of the mammalian Smad-interacting Ski oncoprotein (38, 39). Our present studies highlight how systematic analyses can uncover new connectivities in mammalian signaling pathways, such as that between TGF β receptors and the PAK and polarity networks. Thus, HTP analysis of cell signaling in mammalian cells can begin to unravel how dynamic and highly interconnected signaling networks interpret complex spatio-temporal cues in multicellular organisms.

REFERENCES

1. P. Uetz *et al.*, *Nature* **403**, 623 (2000).
2. A. C. Gavin *et al.*, *Nature* **415**, 141 (2002).
3. T. Ito *et al.*, *Proc Natl Acad Sci U S A* **98**, 4569 (2001).
4. Y. Ho *et al.*, *Nature* **415**, 180 (2002).
5. L. Giot *et al.*, *Science* **302**, 1727 (2003).
6. S. Li *et al.*, *Science* **303**, 540 (2004).
7. K. Miyazono, S. Maeda, T. Imamura, *Oncogene* **23**, 4232 (2004).
8. A. B. Roberts, L. M. Wakefield, *Proc Natl Acad Sci U S A* **100**, 8621 (2003).
9. R. J. Akhurst, R. Deryck, *Trends Cell Biol* **11**, S44 (2001).
10. P. ten Dijke, C. S. Hill, *Trends Biochem Sci* **29**, 265 (2004).
11. Y. Shi, J. Massague, *Cell* **113**, 685 (2003).
12. L. Attisano, J. L. Wrana, *Science* **296**, 1646 (2002).
13. T. Hunter, *Cell* **100**, 113 (2000).
14. T. Pawson, *Cell* **116**, 191 (2004).
15. Material and Methods are available as supporting material
16. I. Stagljar, S. Fields, *Trends Biochem Sci* **27**, 559 (2002).
17. K. Luo *et al.*, *Genes Dev* **13**, 2196 (1999).
18. J. Kawai *et al.*, *Nature* **409**, 685 (2001).
19. N. Przulj, D. A. Wigle, I. Jurisica, *Bioinformatics* **20**, 340 (2004).
20. J. S. Bader, A. Chaudhuri, J. M. Rothberg, J. Chant, *Nat Biotechnol* **22**, 78 (2004).
21. A. L. Barabasi, Z. N. Oltvai, *Nat Rev Genet* **5**, 101 (2004).
22. S. H. Yook, Z. N. Oltvai, A. L. Barabasi, *Proteomics* **4**, 928 (2004).

23. H. Jeong, S. P. Mason, A. L. Barabasi, Z. N. Oltvai, *Nature* **411**, 41 (2001).
24. J. C. Rain *et al.*, *Nature* **409**, 211 (2001).
25. E. Ravasz, A. L. Barabasi, *Phys Rev E Stat Nonlin Soft Matter Phys* **67**, 026112 (2003).
26. E. Ravasz, A. L. Somera, D. A. Mongru, Z. N. Oltvai, A. L. Barabasi, *Science* **297**, 1551 (2002).
27. J. D. Han *et al.*, *Nature* (2004).
28. S. J. Wicks, S. Lui, N. Abdel-Wahab, R. M. Mason, A. Chantry, *Mol Cell Biol* **20**, 8103 (2000).
29. S. Edlund *et al.*, *Mol Biol Cell* **14**, 529 (2003).
30. M. Sultan *et al.*, *Bioinformatics* **18 Suppl 1**, S111 (2002).
31. G. M. Bokoch, *Annu Rev Biochem* **72**, 743 (2003).
32. K. Luettich, C. Schmidt, *Mol Cancer* **2**, 33 (2003).
33. M. C. Wilkes, S. J. Murphy, N. Garamszegi, E. B. Leof, *Mol Cell Biol* **23**, 8878 (2003).
34. W. Chen, M. Yazicioglu, M. H. Cobb, *J Biol Chem* **279**, 11129 (2004).
35. S. Edlund, M. Landstrom, C. H. Heldin, P. Aspenstrom, *Mol Biol Cell* **13**, 902 (2002).
36. L. Gonzalez-Mariscal, A. Betanzos, P. Nava, B. E. Jaramillo, *Prog Biophys Mol Biol* **81**, 1 (2003).
37. B. Ozdamar *et al.*, *submitted* (2004).
38. M. Tewari *et al.*, *Mol Cell* **13**, 469 (2004).
39. L. S. da Graca *et al.*, *Development* **131**, 435 (2004).
40. We thank L. Attisano for critical review and support throughout this project, members of the Attisano and Wrana labs for cDNA reagents, advice and encouragement throughout this project , especially C. Le Roy, S. Bonni, L. Izzi and N. Pece-Barbara, and Etienne Labbé for the Smad subnetwork movie. Work in J.L.W's lab was supported by funds from Genome Canada, the Canadian Institutes of Health Research (CIHR) and the National Cancer Institute of Canada

with funds from the Canadian Cancer Society. Work in IJ's lab is supported by NIH (P50 GM-62413), NSERC and an IBM Shared University Research and IBM Faculty partnership. M.B-R. is a CIHR Postdoctoral Fellow; B.O. and R.B. hold PhD and MD/PhD CIHR studentship, respectively; K.R.B. is supported by a Scholarship from the Institute of Robotics and Intelligent Systems (Precarn Incorporated); N.P. holds an Ontario Graduate Scholarship. J.L.W. is an International Scholar of the Howard Hughes Medical Institute and a CIHR Senior Investigator.

SUPPORTING ONLINE MATERIAL

www.sciencemag.org

Materials and Methods

Figs. S1, S2, S3, S4

Tables S1, S2

Movie S1

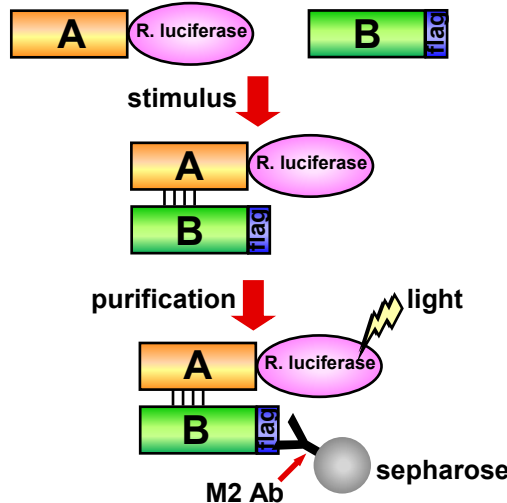
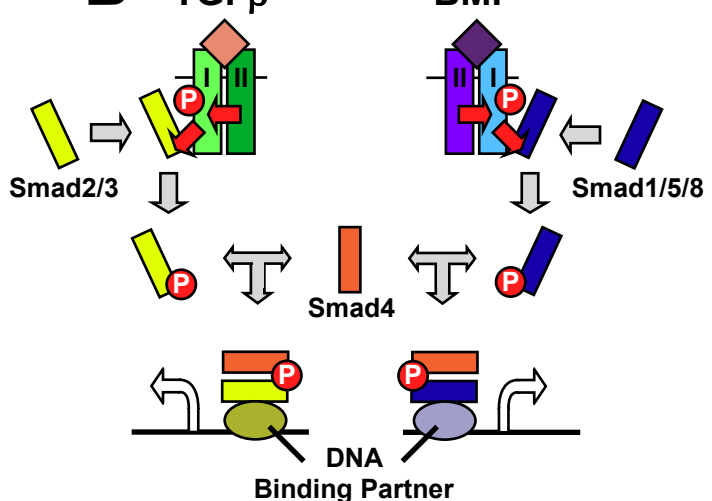
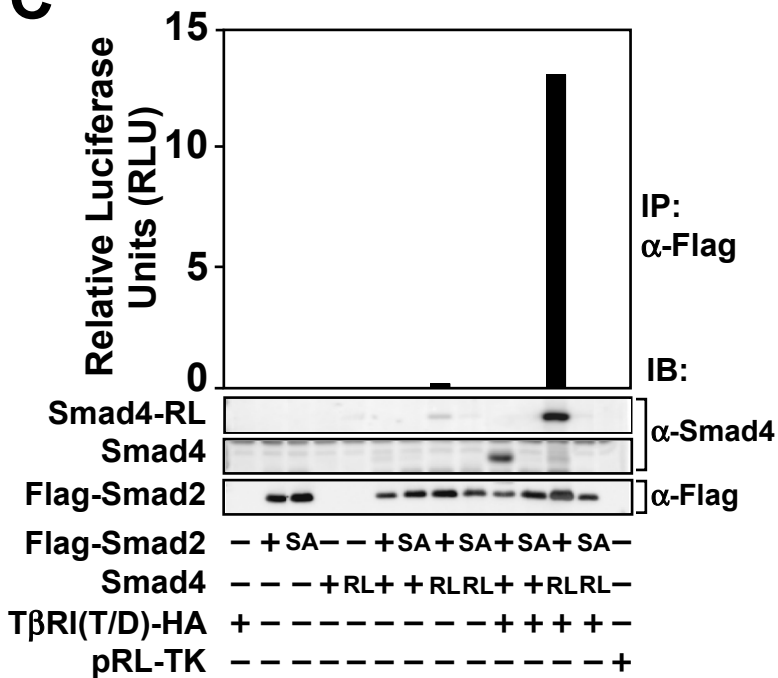
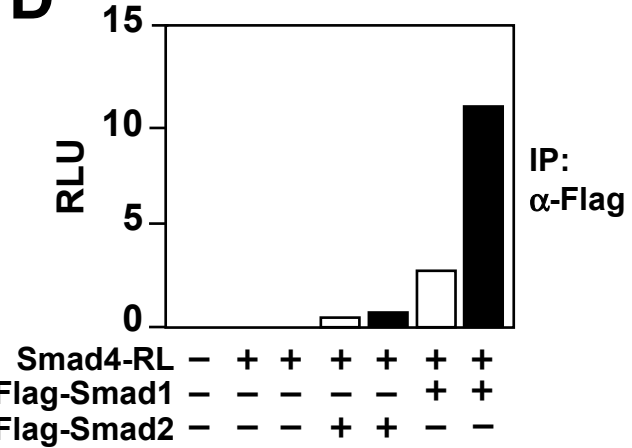
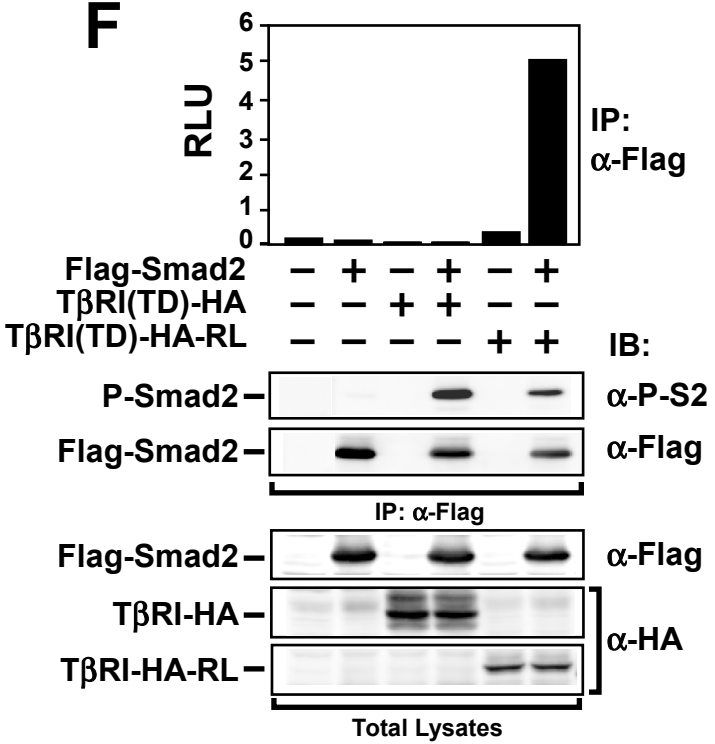
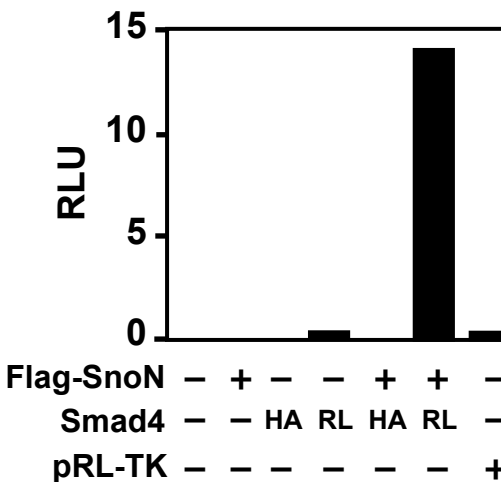
FIGURE LEGENDS

Figure 1. The luminescence-based strategy for the detection of mammalian protein-protein interactions. (A) LUMIER. RL-tagged protein A co-expressed with a Flag-tagged partner B in mammalian cells is detected in immunoprecipitates enzymatically as light emission. (B) Schematic of the TGF β and BMP Smad signaling pathways. See text for details. (C) LUMIER detects phosphorylation-dependent interactions. HEK-293T cells were transfected with wild type or RL-tagged Smad4 together with either wild type (+) or the phosphorylation site mutant (SA) of Flag-Smad2. TGF β signaling (+) was induced by expression of constitutively active T β RI(T/D)-HA. Smad4 interaction with Smad2 was determined by measuring RL activity in anti-Flag immunoprecipitates (histogram; RLU, relative luciferase units) or by immunoblotting (IB) with anti-Smad4 antibody. pRL-TK is RL driven by the thymidine kinase promoter and is a negative control. (D) LUMIER distinguishes signal-specific interactions. HEK293T cells were transfected with Smad4-RL and Flag-Smad1 or Flag-Smad2 in the presence (black) or absence (white) of BMP signaling. Protein interactions in anti-Flag immunoprecipitates were determined by measuring RL activity. (E) Detection of signal-independent interactions by LUMIER. HEK293T cells were transfected with Flag-SnoN and Smad4-RL or Smad4-HA and their association detected as in (D). (F) Detection of T β RI-Smad2 interaction by LUMIER. HEK-293T cells were transfected with constitutively active T β RI(TD)-HA-RL or T β RI(TD)-HA along with Flag-Smad2 and their association detected as in (C) (top panel). Levels of phosphorylated Smad2, total Smad2, and receptors were confirmed by immunoblotting with anti-phosphoSmad2 antibody (α -P-S2), anti-Flag and anti-HA, respectively (lower panels).

Figure 2. High-throughput LUMIER. (A) Pilot screen in 96-well plates. HEK293T cells were transfected with 30 different Flag-tagged cDNAs (indicated), or empty vector (V) and HA-tagged T β RI (T β RI-HA) as negative controls, together with Smad4-RL and interactions assessed by LUMIER in the presence or absence of TGF β signaling. Results are plotted as the mean relative luciferase activity (RLU) \pm SD of triplicates from a representative experiment. (B) Summary of results from the TGF β pathway LUMIER screen. TGF β pathway components (listed on the left), fused to Renilla Luciferase were screened against 518 3Flag-tagged cDNAs in the presence (*) or absence of TGF β signal. Individual cDNAs, identified by numbers at the top of each panel, were grouped by domain composition. Each row corresponds to one pathway component and the LIR score for each test is represented colourimetrically, with the tone of yellow representing the LIR value as defined by the scale on the right. W, wild type, K, kinase-deficient, Q and T constitutively-active, C, catalytically inactive.

Figure 3. The TGF β interactome by LUMIER. (A) Network graph of the TGF β interactome. Proteins are vertices and are color-coded according to their Gene Ontology annotation (inset). Interactions with a LIR of 3 or greater are shown as edges (blue). For clarity, Smads under different signaling conditions and various wild type, activated and catalytically inactive versions of Smurfs and receptors have been condensed into single vertices. (B) Dynamics of the Smad subnetwork. The Smad (MADH2 and 4) network in the absence (left) and presence (right) of TGF β signaling are shown, with the edge colour reflecting the LIR (inset). Note the dynamics of the network (see also Movie S1).

Figure 4. The TGF β receptor connects subnetworks involved in cell motility and polarity. (A) Combined unsupervised and supervised BTVQ clustering identifies a group of proteins with similar SOMs. IRF3 (lower right), which is part of a different cluster, is shown for comparison. (B) Association of Flag-tagged proteins with TGF β receptors. HEK293T cells transiently transfected as indicated, were affinity-labeled and lysates subjected to immunoprecipitation with anti-Flag antibody. Coprecipitating receptors were visualized by autoradiography and the expression of Flag-tagged proteins confirmed by immunoblotting (IB). CHEK and DUSP3 did not interact with T β RI in the LUMIER screen. (C, D) Endogenous PAK1 and Occludin associate with the TGF β receptor. NMuMG cell lysates were subjected to non-immune (NI) or anti-T β RI immunoprecipitation (α T β RI) followed by immunoblotting with anti-PAK1 (C) or anti-Occludin (D) antibodies. The antibody heavy chain is indicated (IgH) (E) Occludin associates with cell surface TGF β receptors. Occludin interaction with TGF β receptors was determined as in (B). (F) The TGF β pathway links the otherwise sparsely connected PAK1 and polarity networks. The connectivity between the PAK1 (blue) and polarity (green) networks is shown before (i) and after (ii) the LUMIER screen with TGF β pathway components (red nodes). Purple nodes are proteins from either network that were present in the LUMIER screen. Nodes connected by black edges represent interactions previously reported in the literature, whereas red edges indicate novel associations unveiled by LUMIER or our directed experiments (see text for details).

A**B****C****D****F****E****Fig. 1 Barrios-Rodiles et al., 2004**

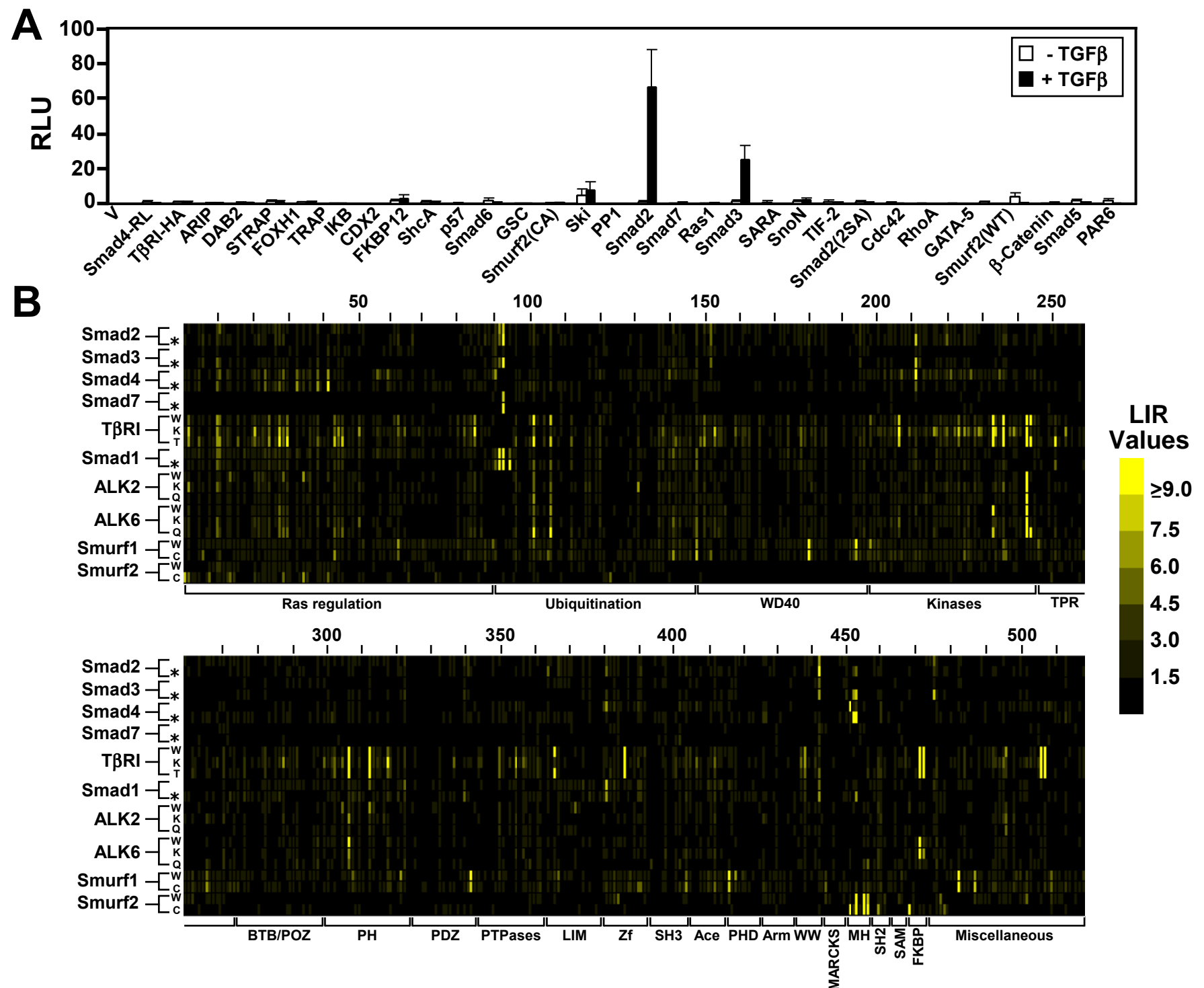


Fig. 2 Barrios-Rodiles et al., 2004

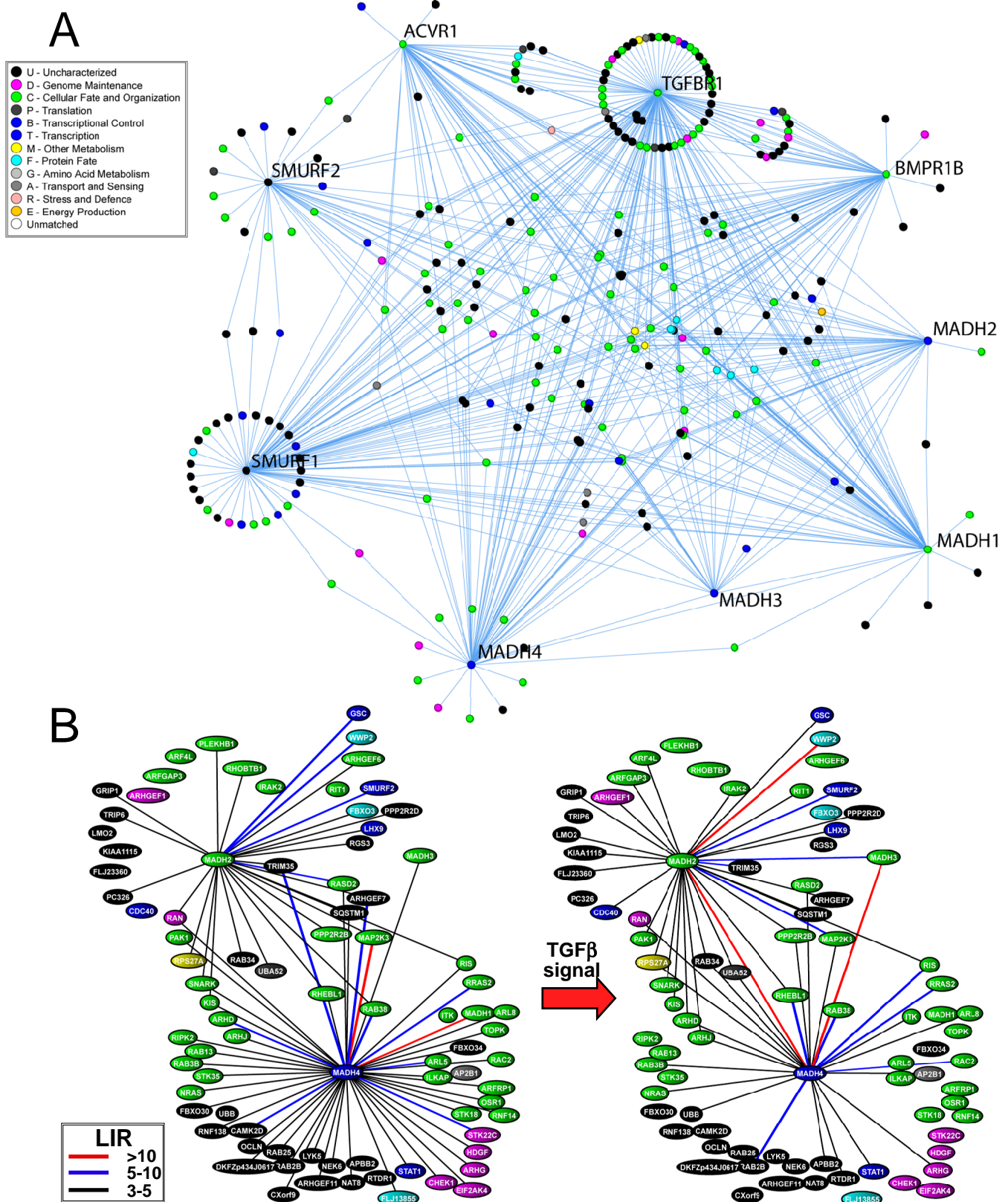


Fig. 3 Barrios-Rodiles et al., 2004

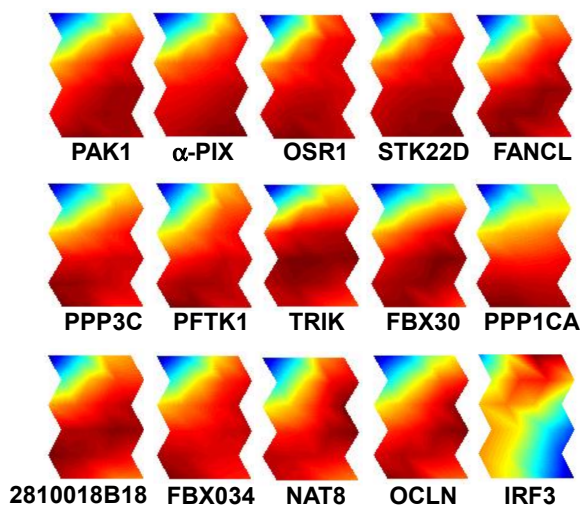
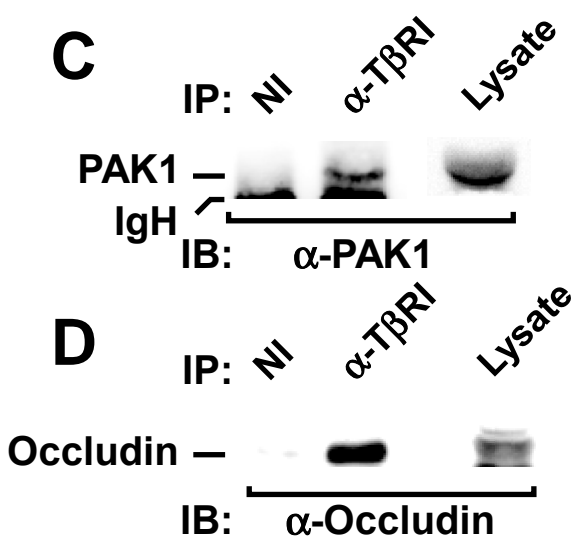
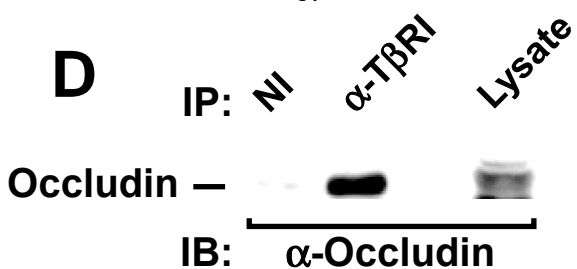
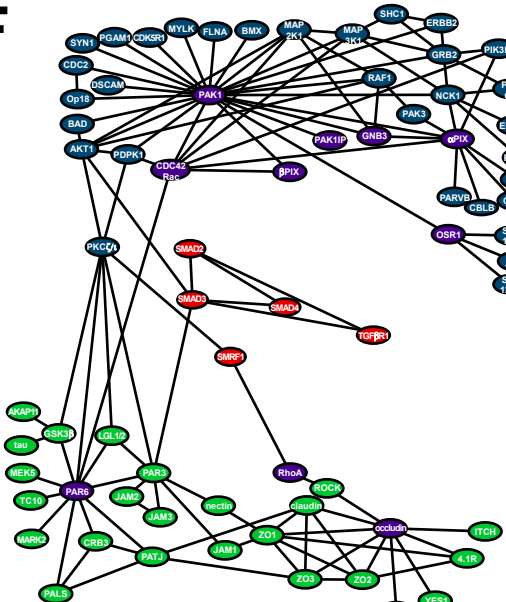
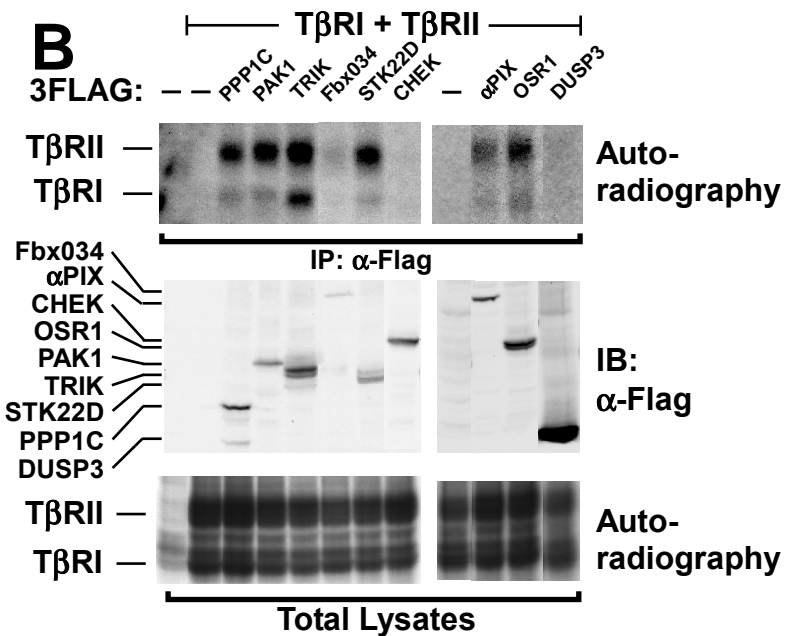
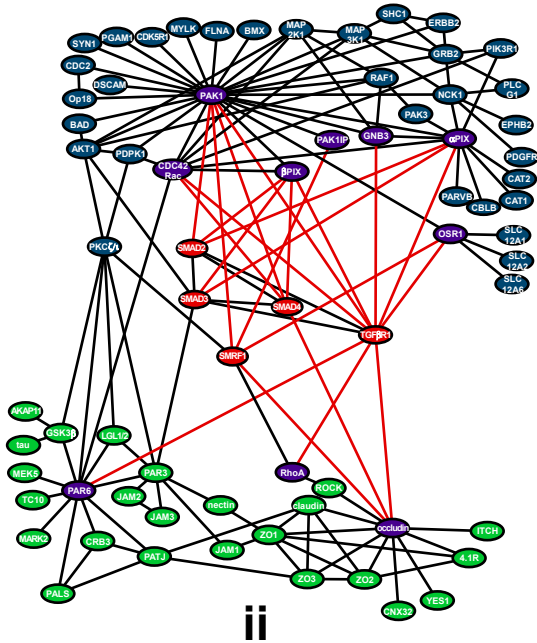
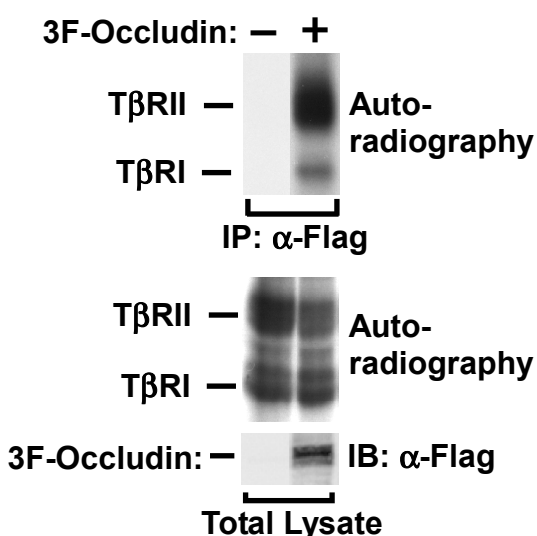
A**C****D****F****i****B****E****ii**

Fig. 4 Barrios-Rodiles et al., 2004

SUPPORTING ONLINE MATERIAL

For:

**High-throughput mapping of a
dynamic signaling network in mammalian cells**

Barrios-Rodiles *et al.*

MATERIALS AND METHODS

Development of LUMIER. HEK293T cells plated in 6-well dishes were manually transfected using the calcium-phosphate precipitation method. After 48 h, cells were lysed as in (1) and then immunoprecipitated using anti-Flag M2 monoclonal antibody (Sigma). Total protein expression was confirmed by immunoblotting with anti-Smad4 (rabbit) and anti-HA (rat, Roche) antibodies. Luciferase activity in immunoprecipitates and in aliquots of total cell lysates was determined using the Renilla Luciferase Assay System (Promega). For adaptation into the 96-well format, a Multiprobe II Ex 4 Tip (Packard) was used for liquid handling procedures.

Construction of the Renilla luciferase-tagged cDNAs. Renilla luciferase tagged baits were generated by PCR, subcloned into pCMV5 and verified by sequencing. Smad4 and TGF β receptor type I (T β RI-HA) were tagged with Renilla luciferase (AF025846), and the others with a humanized version (AF362545). Smad1, 2 and 3, Smurf1 and Smurf2 were amino-terminally tagged while the receptors, Smad4 and Smad7 were tagged at the carboxy-terminus.

Construction of 3Flag-tagged cDNA collection. Approximately 600 cDNAs from the FANTOM1 mouse cDNA library (2) were manually curated to define the longest open reading frames containing identifiable domains involved in cell signaling (Fig. S1 and Table S2) and of these, 95% were successfully amplified using Platinum Pfx polymerase (Invitrogen). The blunt-ended PCR products were purified with the QIAquick gel extraction kit (QIAGEN) and then subcloned into a customized pCMV5-based directional

TOPO-vector (Invitrogen) that included an amino-terminal 3X Flag epitope tag. Eight colonies from each ligation reaction were then screened by PCR and insert orientation and the presence of a stop codon confirmed using a diagnostic EcoRI restriction site incorporated into the reverse primers. DNA from positive colonies was purified using the 96-well format QiaWell kit (QIAGEN). The overall cloning success rate for generating the 3Flag-tagged cDNA set was 77.5%. Twenty-eight in house Flag-tagged cDNAs were included in the set for the screens and can be identified by their Accession numbers in Table S2.

Automated imaging. To confirm expression and to obtain preliminary information on subcellular localization of the 3Flag-tagged proteins (Fig. S2), COS-7 cells plated in 96-well dishes were transiently-transfected with each clone using PolyFect (QIAGEN). After 48 h, cells were fixed, permeabilized and proteins visualized using an anti-Flag M2 antibody followed by AlexaFluor-488 conjugated goat anti-mouse antibody (Molecular Probes). Images were obtained using the high-throughput ArrayScan II System (Cellomics, Pittsburgh, PA). Colonies from confirmed clones were pooled into one well of 96-well plate. Working aliquots (5 μ l) of 3Flag-tagged cDNAs at 0.02 μ g/ μ l were aliquoted into 96-well plates and stored at -80 °C for the LUMIER screens. Detailed information on each 3Flag-tagged cDNA will be made available via the Web upon publication.

LUMIER automation. The screens (Table S1) were carried out on a ThermoCRS (Burlington, ON) Robotic platform. This platform comprises a Robotics Articulated Arm which runs along a 3 m UMI-33 TRACK system (ThermoCRS), and has access to 14 pieces of equipment mounted on a custom designed table. HEK293T cells were plated at

a density of 22,000 per well in poly-D-lysine coated 96-well plates (COSTAR, Corning) in complete DMEM with antibiotics 24 h before transfection. Cells were transiently-transfected with 100 ng of each 3Flag-tagged cDNA and 125 ng of the Renilla luciferase tagged bait diluted in DMEM without serum or antibiotics using PolyFect (QIAGEN). Transfected cells were maintained at 37 °C and 48 h later were lysed as previously described (1). A Multimek 96 (Beckman) liquid handler was used to transfer seventy percent of the cell lysates to a white round-bottom NBS plate (COSTAR, Corning) containing 5 µl of paramagnetic beads (Dynal) coupled to protein G and the monoclonal M2 anti-Flag antibody (Sigma). Immunoprecipitations were carried out for 1 h at 4 °C in a shaker-incubator (ThermoCRS) and the beads washed 8 times using a Biotek ELx405 MAGNA washer with a modified magnetic nest (ThermoCRS). Renilla luciferase activity in the immunoprecipitates was measured in a Berthold Luminometer with the Renilla Luciferase Assay System (Promega). Total expression of the Renilla luciferase-tagged protein was confirmed using ten percent of the cell lysates with the Dual-Glo Luciferase Assay System (Promega) in a CCD camera equipped chemiluminescence imaging plate reader (CLIPR, Molecular Devices, CA).

Biochemical analysis for validation of interactions. For affinity-labeling, HEK293T cells expressing the TGFβ type I and type II receptors along with the 3Flag-tagged cDNAs were incubated with 250 pM [¹²⁵I]-TGFβ in media for 1h at 37°C and receptors then cross-linked to ligand and immunoprecipitated with anti-Flag M2 antibody as described (9). For GST-CRIB pull-down assays, affinity-labeled receptors were collected using GST-CRIB as previously reported (10). Endogenous interactions in mouse

mammary epithelial cells (NMuMG) were detected using anti-T β RI (V22, Santa Cruz), anti-PAK1 (Santa Cruz) and anti-Occludin (Zymed) antibodies.

Data Analysis and Visualization of LUMIER Results

LIR Calculations. To calculate each LUMIER interaction intensity ratio (LIR), the 8 negative control wells on each 96-well plate were averaged. Next, a ratio of the luciferase intensity of each bait (RL-fusions) and prey (3Flag-tagged cDNAs) combination against its corresponding mean negative control was obtained. A linear scaling factor was applied to the LIR dataset for each bait to normalize for experiment-to-experiment variability in luciferase intensity, that is due to variability in total expression levels of RL-tagged proteins. Finally, the LIR's from replicate experiments were averaged to provide the final LIR for each bait-prey combination. To generate a table of all LIR values (Table S2) each 3Flag-tagged FANTOM1 clone was grouped according to its domain as defined by *SMART*. We next performed BLAST analysis using the FANTOM1 sequences and the top scoring E value was used to label each clone. The corresponding mouse and human Unigene IDs for each clone are also provided in Table S2.

LUMIER Assay Performance. LUMIER provides quantitative information regarding protein interactions, which can be used to assess confidence that an interaction is real. To evaluate LUMIER performance we first determined reproducibility of the assay by calculating the Pearson's correlation coefficient for multiple repeated screens of T β RI, Smad2, Smad4 and ALK2. This revealed an average Pearson's correlation of 0.8. As perfect correlation (i.e. identical data in both screens), would be reflected by a score of 1,

this suggests that the screen yields good assay-to-assay reproducibility. Next, we evaluated false negative rates at different LIR cutoffs. For this we comprehensively searched the literature and generated a list of about 500 protein interactions in the TGF β signaling pathway, of which 64 were tested in our LUMIER screen. At a LIR cutoff of 1 (i.e. all positive data points in the screen), the false negative rate was low at 9%. However, at LIR cutoffs of 2 and 3 this rose to 24% and 31%, respectively. False positive rates are difficult to accurately measure as it is hard to prove that two proteins do not interact *in vivo*, however we estimated these rates by examining 31 novel interactions of LIRs over 3, using secondary assays, and observed 5 that were not reproducible. This yielded an approximate false positive rate of 16% for LIRs over 3. Furthermore, when we examined the number of statistically significant hits as a function of the LIR cutoff we observed that the ratio of statistically significant to insignificant interactions at a *p* value < .05 was 18%, whereas at a LIR of 2 it climbed markedly to 48%. Therefore, for building the network graph we used a conservative LIR cutoff of 3, which yields a high quality PPI dataset. LUMIER thus delivers high confidence interaction data that compares very favourably to HTP Y2H screens, which are known to produce high rates of false negative (>70%) and false positive interactions (3, 4). Interactions with LIR cutoffs of 3 were integrated into a network, and visualized using a custom Java-based application (Fig. 3A). Network dynamics (Fig. 3B) were represented using a modification of the *Spring-Embedder* algorithm, whereby edge lengths were made inversely proportional to the LIR score and the final network adjusted manually to aid visualization of nodes. Edges in the dynamic network were then colour coded to reflect LIRs.

Network Analysis. The network generated at LIR cutoff of 3 has 901 protein interactions amongst 276 proteins. The degree distribution of the network followed a power-law distribution and appears scale-free (Fig. S3A). Furthermore, the $C(k)$ clustering coefficient of degree k proteins scales as k^{-1} (Fig. S3B), indicating the network's hierarchical modularity. The diameter of the network, that is, the average of shortest path lengths over all pairs of nodes, is 2.8, which is close to $\log(n)$, indicating the small-world nature of the network. These features of the TGF β network are similar to those displayed by other PPI networks (5), as well as other biological (6) and real-world networks (7).

Unsupervised clustering using BTSVQ. To identify biologically meaningful information from our PPI dataset, we employed Binary Tree-Structured Vector Quantization (BTSVQ), which combines tree-structured vector quantization and partitive k -means clustering (8). BTSVQ provides robust unsupervised clustering that is resilient to data preprocessing and normalization, and can extract biologically meaningful clusters from complex datasets. BTSVQ combines self-organizing maps (SOM) and partitive k -means clustering in a complementary fashion. The algorithm can be used for high-dimensional data clustering and visualization, both of preys and baits. To cluster preys, the algorithm partitions data using the standard k -means algorithm in prey space, where k is kept constant at 2. Iteratively applying the algorithm and using evaluation of variance as a stopping criterion, it generates a binary tree. The SOM algorithm is then used to cluster the bait space. This yields SOMs in which each component plane represents one of the 3Flag-tagged proteins used in the screen and the map unit colour reflects the relative LIR values for that protein (that is, the interaction profile of a particular protein

with TGF β pathway components) (see Fig. 4A). For each level of the binary tree, the preys are then ranked both with respect to quantization error, which is the likelihood of the prey having differential interaction affinity across all baits in the same cluster, and t -statistics. This provides an accurate method of excluding baits with variable interaction affinity across preys, as well as baits with low significance, and thus enables selection of the most differentiating baits between clusters. The cluster structure in prey space is visualized using component planes of the already computed SOM and preys displaying similar patterns sorted for validation.

References for Supplementary Material

1. P. A. Hoodless *et al.*, *Cell* **85**, 489 (1996).
2. J. Kawai *et al.*, *Nature* **409**, 685 (2001).
3. A. J. Walhout *et al.*, *Science* **287**, 116 (2000).
4. M. Tewari *et al.*, *Mol Cell* **13**, 469 (2004).
5. S. H. Yook, Z. N. Oltvai, A. L. Barabasi, *Proteomics* **4**, 928 (2004).
6. E. Ravasz, A. L. Somera, D. A. Mongru, Z. N. Oltvai, A. L. Barabasi, *Science* **297**, 1551 (2002).
7. E. Ravasz, A. L. Barabasi, *Phys Rev E Stat Nonlin Soft Matter Phys* **67**, 026112 (2003).
8. M. Sultan *et al.*, *Bioinformatics* **18 Suppl 1**, S111 (2002).
9. T. Tsukazaki, T. A. Chiang, A. F. Davison, L. Attisano, J. L. Wrana, *Cell* **95**, 779 (1998).
10. E. Vignal *et al.*, *J Biol Chem* **275**, 36457 (2000).
11. C. Cifuentes-Diaz *et al.*, *Muscle Nerve* **29**, 59 (2004).
12. C. Albertinazzi, A. Cattelino, I. de Curtis, *J Cell Sci* **112 (Pt 21)**, 3821 (1999).
13. P. J. Peters *et al.*, *J Cell Biol* **128**, 1003 (1995).

Figure Legends for Supplemental Material

Figure S1. Construction of the 3Flag-tagged cDNA collection. Manually curated FANTOM1 cDNA clones were amplified by PCR. An example of 96 PCR reactions is shown. The purified bands were subcloned into the customized 3Flag-pCMV5 TOPO vector. Directionality in the vector is provided by the underlined GTGG overhang which hybridizes with the CACC (in red) from the PCR product. The EcoRI site (in magenta) was included in the reverse primer to confirm the presence of the stop codon. Eight colonies per clone were screened by PCR followed by EcoRI digestion. Only cDNAs containing inserts with the stop codon and in the correct direction were subjected to the expression screen by immunofluorescence in COS-7 cells. Six colonies from the same clone, displaying similar subcellular localization are shown. Expressing colonies from the same clone were pooled to perform the LUMIER screens.

Figure S2. Subcellular localization of the 3Flag-tagged set of cDNAs in mammalian cells. COS-7 cells expressing 3Flag-tagged cDNAs were immunostained with anti-Flag M2 antibody followed by AlexaFluor 488-conjugated goat anti-mouse. **(A)** Hypothetical protein, MGC 2941, with a PHD domain localized to the nucleus. **(B)** Myoneurin, containing BTB and zfC2H2 domains, localized to specific nuclear regions as reported (11). **(C)** Rac1 expressing cells showed an increased number of filopodia (12). **(D)** FBOXO30 containing a F-box domain is localized to the cytosol. **(E)** A BTB and Kelch domain containing hypothetical protein, SBB126, displayed a punctate cytosolic pattern. **(F)** ADP-ribosylation factor 6 localized to the plasma membrane as previously shown (13).

Figure S3. Network Graph Parameters. (A) Degree distribution of the TGF β network.

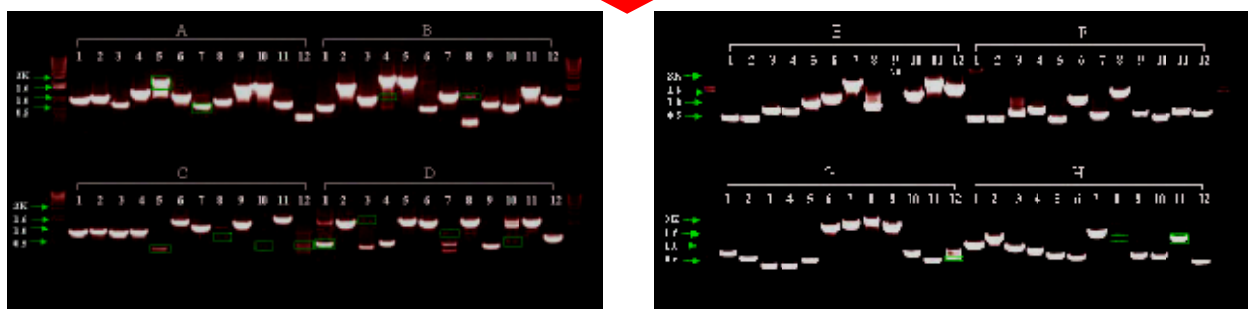
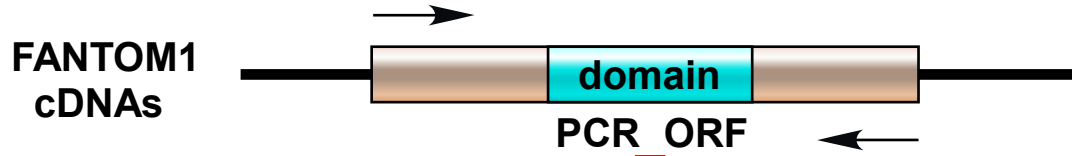
The Probability of proteins with degree k ($P(k)$) is plotted against their degree (k) in a log-log graph. The connectivity of the nodes in the network roughly follows a power-law (scale-free) with an exponent of 1.7. (B) Clustering coefficient of the network. The average clustering coefficient is shown as a function of all nodes of degree k in the network. $C(k)$ approximately follows $C(k) \sim k^{-1}$ as shown by the fitted line in the graph.

Figure S4. Association of TGF β receptor complexes with members of the PAK1

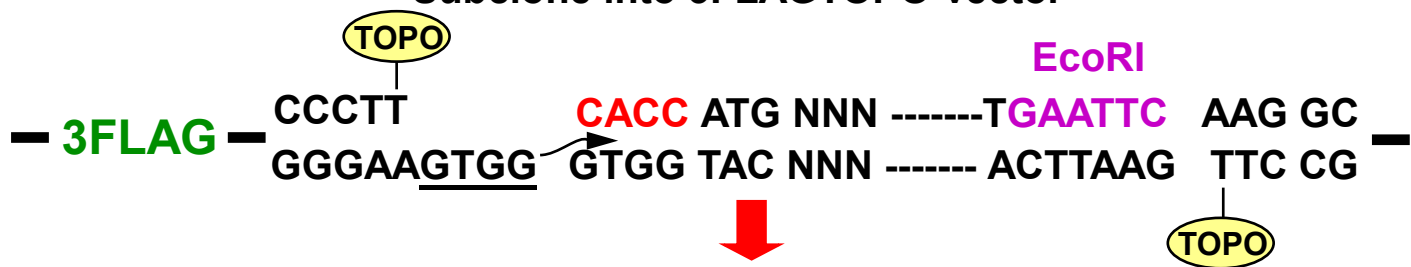
subnetwork. HEK293T cells were transiently-transfected with wild type or kinase-deficient (KR) TGF β type I and type II receptors and the indicated Flag-tagged constructs. Cells were affinity-labelled with [125 I]-TGF β and cell lysates subjected to anti-Flag immunoprecipitation (A and B) or to GST-CRIB affinity purification (C). (A) β -PIX associates with the TGF β type II receptor and the TGF β receptor complex. (B) Cdc42 associates with the TGF β receptor complex. (C) TGF β receptors may bind active Cdc42. Cell lysates were subjected to GST-CRIB pulldown to allow isolation of proteins associated with GTP-bound versions of Cdc42.

Movie S1 Dynamics of the Smad subnetwork in the absence and presence of TGF β

signalling. The movie shows the Smad2-Smad4 network in the absence and presence (+TGF β) of TGF β signalling. The distance between nodes is inversely proportional to the LIR value that is also shown by the colour of the edge.



Subclone into 3FLAGTOPO-vector

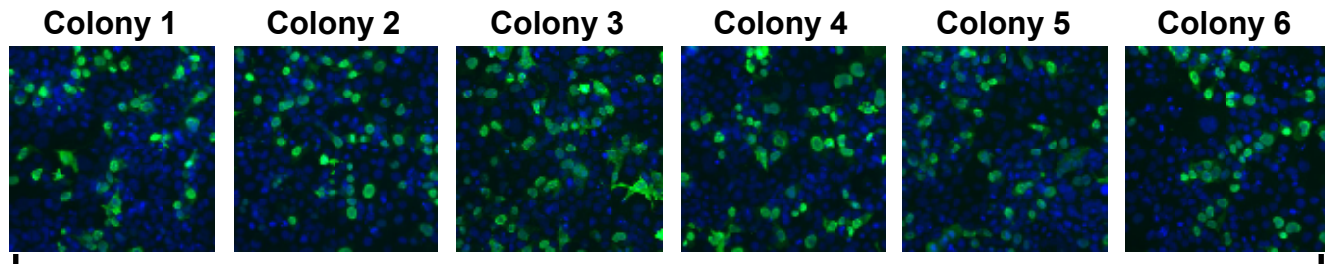


Pick 8 colonies per clone

PCR and EcoRI digestion screen

Select inserts with correct orientation

Immunofluorescence screen

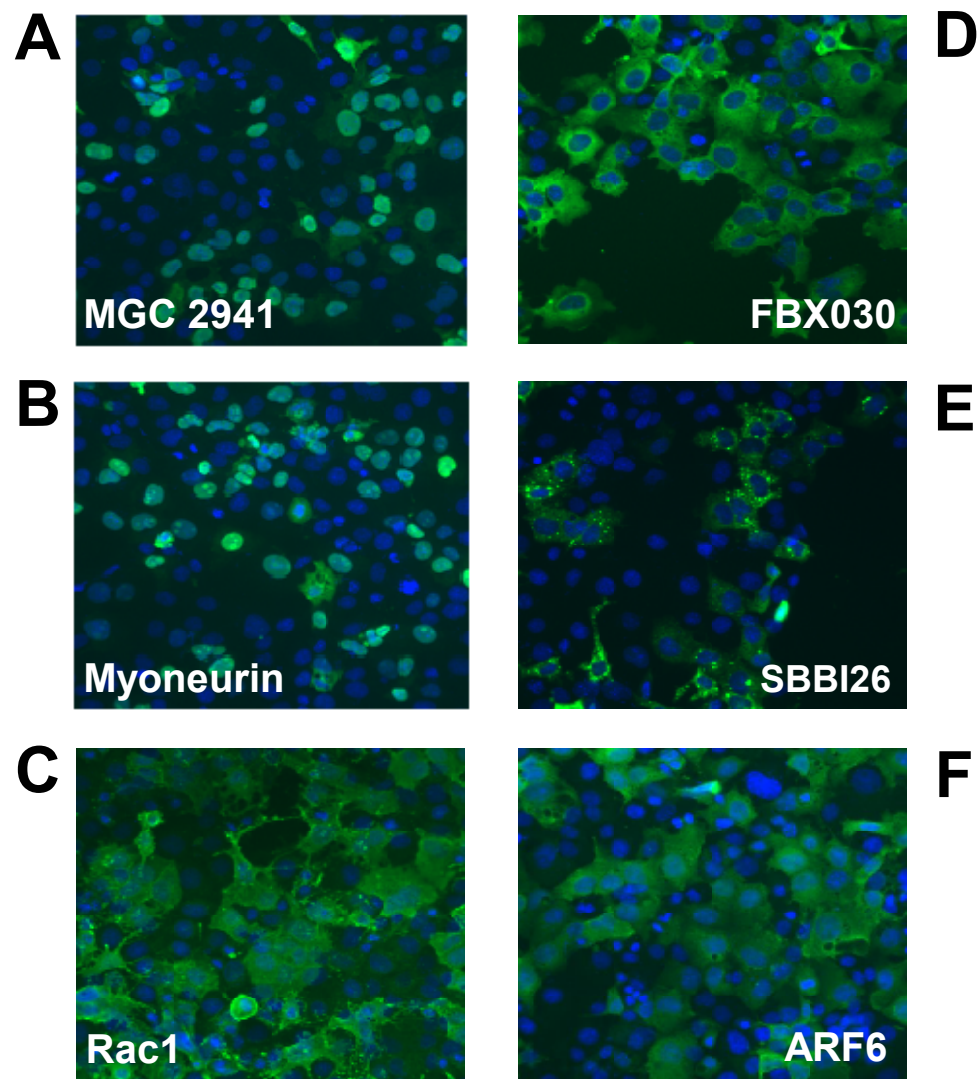


Clone ING1L

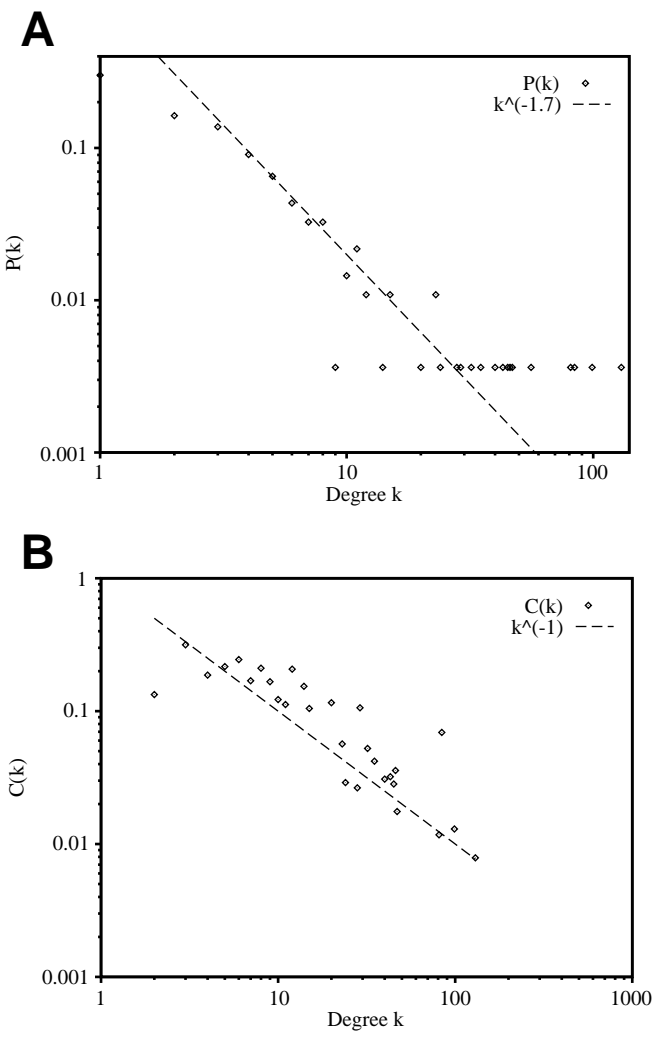
Pool expressing colonies

3FLAG cDNA set

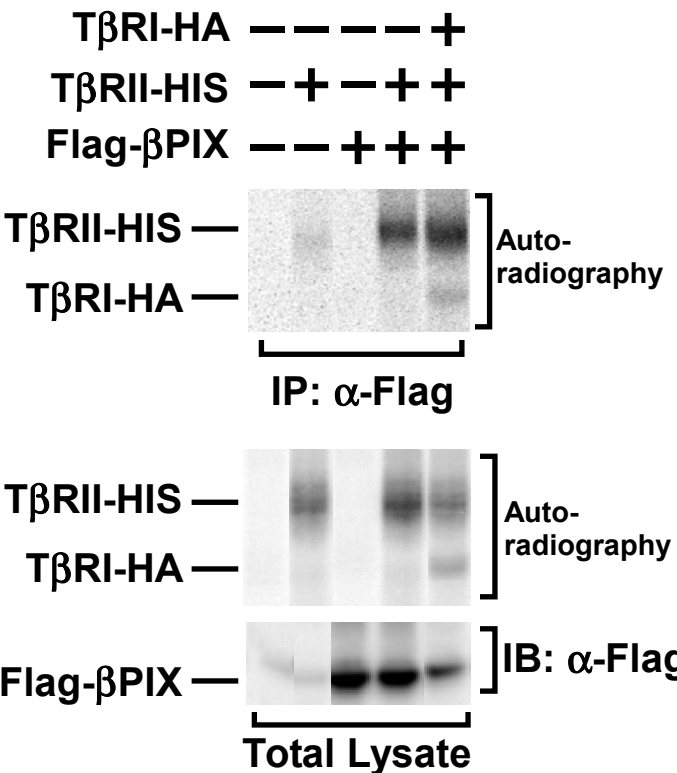
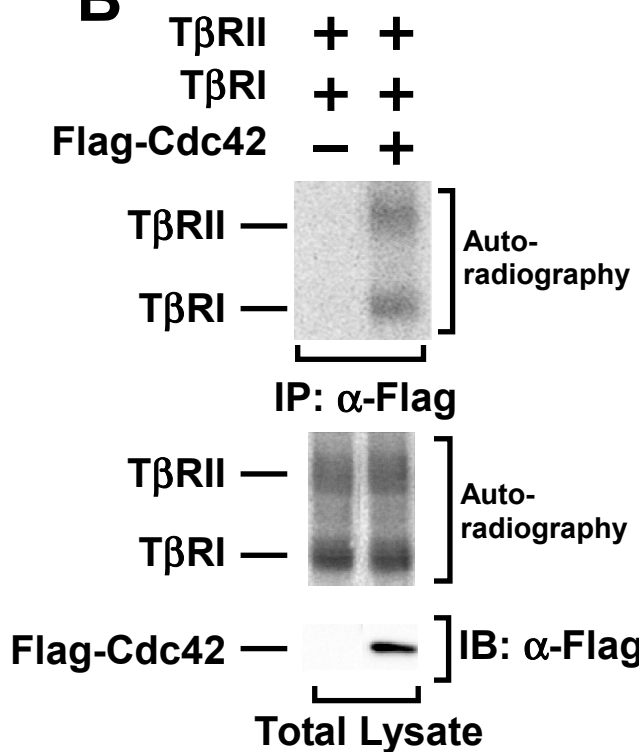
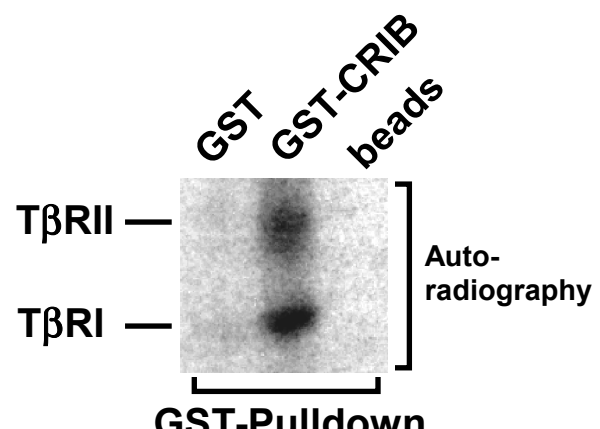
Supplemental Fig. S1 Barrios-Rodiles et al., 2004



Supplemental Fig. S2 Barrios-Rodiles et al. 2004



Supplemental Fig. S3 Barrios-Rodil et al., 2004

A**B****C**

Supplemental Fig. S4 Barrios-Rodiles *et al.* 2004

Table S1: LUMIER screens performed.

Screen	UniGene ID	Interaction partners for positive control
Smad1	Hs. 388294	Smad1+ Flag-Smurf2 (C/A)
Smad1+ BMP	Hs. 388294	Smad1+ Flag-Smurf2 (C/A)
Smad2	Hs. 110741	Smad2+ Flag-Ski
Smad2+TGF- β	Hs. 110741	Smad2+ Flag-Ski
Smad3	Hs. 288261	Smad3+ Flag-Ski
Smad3+TGF- β	Hs. 288261	Smad3+ Flag-Ski
Smurf1 WT	Hs. 436249	Smurf2 (C/A)+ Flag-Smad1
Smurf1 C699A (catalytically inactive)	Hs. 436249	Smurf1(C/A)+ Flag-Smad1
Smurf2 WT	Hs. 438968	Smurf2 (C/A)+ Flag-Smad7
Smurf2 C716A (catalytically inactive)	Hs. 438968	Smurf2 (C/A)+ Flag-Smad7
Smad4	Hs. 75862	Smad4+ 3FlagSmad2+ T β RI(T/D)
Smad4+TGF- β	Hs. 75862	Smad4+ 3F-Smad2+ T β RI(T/D)
Smad7	Hs. 370849	Smad7+ Flag-Smurf2 (C/A)
Smad7+TGF- β	Hs. 370849	Smad7+ Flag-Smurf2 (C/A)
T β RI WT	Hs. 28005	T β RI (WT)+ Flag-FKBP12
T β RI (K232R)	Hs. 28005	T β RI (K/R) + Flag-FKBP12
T β RI (T204D)	Hs. 28005	T β RI (T/D) + Flag-FKBP12
ALK2 WT	Hs. 150402	ALK2 (WT)+ T β RI-Flag
ALK2 (K235R)	Hs. 150402	ALK2 (K/R)+ T β RI-Flag
ALK2 (Q207D)	Hs. 150402	ALK2 (Q/D)+ T β RI-Flag
ALK6 WT	Hs. 87223	ALK6 (WT)+ Flag-FKBP12
ALK6 (K231R)	Hs. 87223	ALK6 (K/R)+ Flag-FKBP12
ALK6 (Q203D)	Hs. 87223	ALK6 (Q/D)+ BMPRII-Flag

The TGF- β and BMP pathways were activated by overexpressing the T β RI (TD) and ALK2 (QD) receptors respectively.

Supplemental Table S1 Barrios-Rodiles *et al.* 2004

Table S2

Table S2

2610313E07	Ras regulation	FLJ10702	Mm.271178	Hs.277255	2.4059	2.0669	1.497	0.7774	2.4807	2.1792	0.571	0.8103	3.1315	2.0986	2.6795	2.756	1.381	0.949	1.4783	1.627	1.548	1.4939	1.548	1.977	1.9652	0.9511	0.864	
1110036H21	Ras regulation	ARF4L	Mm.266840	Hs.183153	2.5999	3.1742	2.175	0.9877	1.9	1.3265	0.487	0.5382	5.2463	5.7592	3.9621	3.31	1.5707	1.056	2.6307	1.747	2.282	2.4694	2.29	7.11	5.7435	1.2549	0.724	
2310008D22	Ras regulation	ARL1	Mm.291247	Hs.372616	1.3934	0.9287	2.12	0.4367	2.15	2.3597	0.583	0.4946	1.4817	2.0071	2.1578	2.345	0.8589	1.385	1.189	1.495	1.563	1.3355	1.234	1.994	1.3662	1.2188	0.558	
5830420E16	Ras regulation	GIT2	Mm.195632	Hs.418057	0.9221	0.7104	1.141	0.252	1.013	0.7752	0.995	0.8332	2.7998	4.6594	2.7096	1.828	0.8208	1.469	1.948	1.698	1.335	1.2948	1.526	2.069	1.2721	1.8867	0.545	
4921525H11	Ras regulation	SMAP1	Mm.196452	Hs.410882	1.2703	1.2298	1.783	0.2418	1.0384	1.7833	0.784	1.1658	0.42	0.724	0.9517	1.317	0.6909	0.931	0.7152	1.25	1.262	1.3084	1.466	1.833	0.9072	1.8239	3.175	
1810004P07	Ras regulation	ARFGAP3-v	Mm.286911	Hs.13014	1.9136	3.3156	1.588	0.7154	1.9274	2.2164	0.305	0.5115	1.6325	1.6321	1.1687	1.811	0.9889	1.343	2.0251	1.718	1.458	1.2821	0.904	2.108	1.8666	0.0766	1.398	
1200003G10	Ras regulation	GNAI3	Mm.271703	Hs.73799	1.3284	1.1426	1.409	0.3505	0.7515	0.9947	0.343	0.5321	1.3596	1.7273	1.462	1.793	0.8552	0.79	1.2749	1.002	1.29	1.2169	1.212	2.075	2.2289	0.793	0.946	
2610200H14	Ras regulation	GNA13	Mm.193925	Hs.9691	1.142	0.8973	1.272	0.3757	0.9214	0.9629	0.214	0.8695	1.344	3.1227	1.2756	1.807	1.0016	0.959	1.5076	1.23	1.025	1.073	1.097	2.836	2.2766	1.3452	0.817	
0610037B21	Ras regulation	GNG11	Mm.25547	Hs.83381	1.0422	0.9689	0.9	0.4088	1.3432	1.1655	0.935	1.1779	1.8001	1.5667	2.7634	1.705	0.9523	1.626	1.417	1.54	1.143	1.2779	0.941	3.438	2.7196	1.4803	1.003	
A930015K11	Ras regulation	GNGT1	Mm.95398	Hs.73112	1.0225	0.9546	1.332	0.2922	1.9597	1.5051	0.199	0.7353	0.9772	1.1278	0.7482	1.359	0.8313	1.252	0.9031	1.215	0.819	0.8206	0.83	2.215	1.9136	1.5649	0.873	
1500031D04	Ras regulation	GNG13	Mm.218764	Hs.247888	0.8532	0.7853	0.922	0.2065	1.3322	1.3876	0.859	1.0198	0.6495	1.5492	0.631	1.377	0.605	1.001	1.0749	1.528	1.042	1.0196	1.322	2.473	1.4636	1.6216	0.768	
2410018N20	Ras regulation	GNGT2	Mm.46299	Hs.181781	1.0997	0.8256	0.755	0.2768	1.7884	2.0047	0.171	1.05165	0.7695	0.7252	0.8503	1.667	0.9358	1.535	0.7117	1.491	0.865	0.855	0.7537	0.785	2.028	1.2573	2.4382	1.411
1110008BL10	Ras regulation	GNG2	Mm.41737	Hs.112928	0.9315	1.2227	1.389	0.3039	0.9134	1.9097	0.89	1.2359	1.3928	1.9539	1.3414	2.127	0.6543	1.255	1.1553	1.528	1.149	1.2618	1.11	2.015	0.8865	1.2132	3.545	
1190002P14	Ras regulation	GNG3	Mm.273707	Hs.179915	1.0072	1.2465	1.145	0.2554	1.2605	1.8086	0.472	0.861	1.4714	2.2996	1.3917	0.94	0.6431	1.161	1.2779	1.388	1.031	1.0577	0.685	1.939	1.4307	0.826	2.376	
1600029K01	Ras regulation	GNG12	Mm.13080	Hs.8107	0.9431	1.4501	0.887	0.3543	0.7201	1.1158	0.398	0.3991	1.1936	1.0702	1.0038	1.114	0.7865	0.693	0.7877	1.116	0.879	0.6114	0.835	2.775	1.9962	0.8186	0.797	
0710005M12	Ras regulation	M1.254898	Mm.443810	Hs.14538	1.0469	1.461	0.2907	0.7814	1.658	0.674	0.6857	0.787	0.8416	0.6155	1.0521	1.4404	0.7292	1.111	0.554	0.7969	0.325	2.035	1.4404	0.7532	1.123			
5830418G11	Ras regulation	RALGPS1A	Mm.2724249	Hs.438242	1.4451	0.9795	0.905	0.3242	1.3462	2.407	0.677	0.6482	1.5461	2.0949	1.0301	1.68	1.1166	1.088	1.4372	1.334	0.686	1.2	1.18	2.841	1.6499	1.0507	1.369	
1300003D20	Ras regulation	RGL3	Mm.110594	Hs.375142	0.4382	0.4515	0.584	0.1181	0.2201	0.3863	0.297	0.2661	0.3945	0.518	0.3924	0.857	0.3951	0.772	0.4682	0.923	0.589	0.5589	0.409	1.559	0.7924	0.0596	0.458	
5830477L08	Ras regulation	CDGAP	Mm.268397	Hs.300670	1.1031	1.0363	1.005	0.3411	0.9652	1.0346	0.513	0.6252	3.1526	3.5135	2.6372	2.125	1.076	1.866	1.9068	1.9054	2.159	3.351	1.7035	0.8827	1.222			
3110043J09	Ras regulation	3110043J09	Mm.128441		1.2889	2.1107	0.353	0.4077	0.999	0.9469	0.395	0.4608	0.7744	0.9704	0.9069	1.331	0.7461	0.964	0.6975	1.055	0.66	0.8223	0.724	1.949	1.4462	0.9779	2.382	
1700026N20	Ras regulation	CHN2	Mm.253127	Hs.407520	1.9979	1.0366	1.5771	0.5435	2.0559	1.3153	0.516	0.9747	5.71	5.1969	3.0727	1.754	1.0568	1.6051	2.126	1.937	1.206	1.8868	1.702	2.088	2.2734	1.0551	1.341	
1200004L23	Ras regulation	INPP5B	Mm.296202	Hs.449942	2.2707	1.1925	1.695	0.4807	2.0026	2.0238	0.608	0.8103	1.5976	1.7344	1.6203	1.635	1.0673	2.235	1.7514	2.128	1.389	1.5269	1.625	2.819	3.2128	1.3763	1.32	
513340C09	Ras regulation	BCR	Mm.182202	Hs.446394	2.1742	1.8135	1.43	0.5138	2.2536	0.9357	0.476	0.6204	3.9524	3.8913	3.2017	2.743	1.7551	2.154	2.5465	2.417	2.966	1.9139	3.663	2.736	2.2766	0.8242	0.521	
0710001E19	Ras regulation	CHN1	Mm.257073	Hs.38018	1.5637	1.2306	1.721	0.3829	2.8746	2.0934	1.199	0.1057	6.0254	12.129	5.4446	1.571	0.9179	3.145	4.2481	2.384	2.054	2.5101	3.724	2.198	1.6048	1.1821	0.991	
493314B03	Ras regulation	ARHGAP19	Mm.21646	Hs.80305	1.6195	1.5796	1.319	0.5476	1.2172	1.571	0.58	0.5998	0.9645	0.7124	0.9022	1.344	0.8522	1.182	1.3192	1.388	1.02	1.2186	1.067	2.583	2.503	0.7532	1.93	
1700006A11	Ras regulation	1700006A11	Mm.158761		1.2492	0.8318	1.512	0.3667	1.3945	1.7347	0.87	1.1864	2.2972	2.5257	1.5098	1.468	0.8544	1.917	1.5005	2.502	1.47	1.5921	4.362	1.93	1.6016	0.7924	0.875	
2610528A06	Ras regulation	ARHGEF1	Mm.3181	Hs.278186	2.4346	3.1764	0.969	2.6279	2.7446	2.2623	0.679	0.8066	1.0766	1.5264	1.4212	1.751	0.9792	1.032	1.6186	2.073	1.1686	2.051	0.8511	0.725	3.68	3.0168	3.4342	0.462
4833419J07	Ras regulation	ARHGAP18	Mm.276368	Hs.413282	1.7823	2.1777	0.803	1.1682	2.7158	1.3412	1.238	1.092	1.3883	2.5859	0.9658	2.106	1.6648	1.121	1.8121	1.322	1.316	2.144	2.8105	1.2082				
KIAA0380	Ras regulation	1110005M11	Mm.179723	Hs.371602	2.1216	1.9894	1.988	1.75	3.0952	1.3676	1.665	1.3097	1.8207	1.2628	1.018	1.596	1.5527	1.1691	1.0549	1.283	4.606	1.9033	1.2661	1.091				
NM_14573	Ras regulation	ARHGEF7	Mm.244068	Hs.172813	3.1998	3.3825	3.481	3.8657	6.2677	2.6003	0.728	0.901	1.1694	1.3178	1.0776	4.226	5.3483	1.239	1.0032	1.404	1.132	1.2788	0.839	2.689	3.6265	0.7812	1.63	
AY014180	ubiquitination	SMURF2-W	Mm.200086	Hs.438968	6.3648	5.8177	1.497	5.9885	0.6733	0.7359	0.642	0.751	0.6355	0.6401	1.338	27.601	26.97	0.91	0.6845	0.824	1.25	0.7122	0.463	1.34	0.9697	1.3601	0.893	
AY014180	ubiquitination	SMURF2/C	Mm.200086	Hs.438968	6.3728	9.8934	2.277	13.017	0.8686	1.1253	8.813	9.0652	0.9129	0.7583	0.7244	32.463	67.005	1.05	0.9045	1.146	1.52	1.0196	1.3101	1.3237	0.978	1.514		
XM_166483	ubiquitination	SMURF1-W	Mm.27735	Hs.436249	0.6379	0.8581	0.476	0.492	2.082	2.0883	0.132	0.1862	0.5638	0.346	0.8391	1.182	0.9538	0.986	0.4719	0.75	0.678	0.6436	1.685	1.343	1.0439	0.79		
XM_166483	ubiquitination	SMURF1-C	Mm.27735	Hs.436249	1.5167	2.7873	0.637	1.4574	0.503	0.5212	0.665	0.5321	0.5697	0.4261	0.6494	5.601	14.48	0.834	0.8631	0.827	0.6731	1.729	1.1509	0.887	1.309			
4930511O11	ubiquitination	4930511O11	Mm.158518		1.3689	0.9132	0.971	0.6063	0.9184	2.0309	1.286	0.7643	1.0415	2.0814	1.8211	2.096	0.9134	1.6081	1.5088	1.515	1.181	1.4761	1.622	2.816	1.5887	0.658	2.024	
4931431F19	ubiquitination	4931431F19	Mm.158518		1.6368	0.9132	0.971	0.6063	0.9184	2.0309	1.286	0.7643	1.0415	2.0814	1.8211	2.096	0.9135	1.6069	1.5085	1.511	1.173	1.4761	1.622	2.816	1.5887	0.658	2.024	
3110003A22	ubiquitination	LOC137886	Mm.41643	Hs.155572																								

Table S2

3010034A12	ubiquitination	FBX30	Mm.220327	Hs.321687	1.7849	1.7632	1.857	1.5022	2.6391	1.6712	1.759	1.4294	2.9522	3.9448	4.0896	2.436	3.0286	2.236	4.2842	2.527	2.85	3.9303	2.583	3.153	2.5571	1.5406	0.751	
2810025M06	ubiquitination	FBXL12	Mm.24608	Hs.12439	2.5437	2.624	1.696	1.8159	0.8118	0.5432	1.064	0.7897	4.4033	4.5087	3.596	3.672	3.2743	1.362	1.5572	1.807	2.224	2.4855	2.124	2.47	2.3011	1.5251	0.799	
261051F120	ubiquitination	MGC15482	Mm.218350	Hs.194948	0.7633	1.0726	1.773	0.9158	1.5235	2.1621	1.38	1.8793	0.8851	2.048	1.7011	1.181	1.0531	1.694	2.8187	1.284	1.671	1.3186	0.314	1.104	1.3611	1.3346	0.153	
1700026A16	ubiquitination	FBXO30	Mm.276229	Hs.421095	1.4291	1.4474	1.806	1.9039	4.7841	2.8121	1.259	1.3569	1.1696	2.5504	2.1902	3.14	2.2533	1.703	3.7661	1.542	1.93	2.5279	2.475	2.054	3.1812	0.9804	1.654	
1200002G09	ubiquitination	FBXO3	Mm.143768	Hs.406787	3.3361	1.8829	1.761	3.3798	2.1116	1.2482	1.257	1.5709	1.9456	3.1853	3.4772	4.591	3.2175	1.453	2.6638	1.42	3.991	5.1201	3.303	4.428	7.1117	0.7675	0.143	
5830426G16	ubiquitination	FBXO34	Mm.11935	Hs.15467	1.332	1.54	1.272	1.6116	3.021	1.2855	1.008	1.1864	2.4821	2.9252	4.9083	2.373	2.1017	2.162	2.1295	2.138	2.212	2.2196	2.657	2.663	2.6558	0.8572	0.08	
4933422D21	ubiquitination	FBXO24	Mm.158603	Hs.283764	2.5785	1.8198	1.77	2.1141	1.7202	1.0297	1.396	0.9989	2.7443	2.8896	4.2732	4.088	2.9479	2.015	2.1068	2.237	2.878	3.4391	2.183	4.113	4.0459	1.0458	0.114	
6430603C09	ubiquitination	Skp1a	Mm.42944	Hs.488433	1.1843	1.6713	1.793	1.8351	2.2083	0.7884	1.473	0.9977	0.9072	1.2526	1.5276	2.483	1.6528	1.235	1.0057	0.953	1.667	1.1416	1.202	2.035	1.5951	0.8933	0.309	
4932411N15	ubiquitination	CUL2	Mm.291707	Hs.82919	1.0817	1.1898	0.644	1.518	1.6068	0.8716	0.943	0.439	1.7439	1.784	2.1095	2.485	1.5752	1.96	2.6279	1.573	2.275	1.8089	1.334	2.24	2.9885	0.8105	0.232	
8430423K24	ubiquitination	CUL5	Mm.218910	Hs.440320	1.2404	0.9864	0.354	1.1874	2.3626	1.4376	0.895	0.8659	1.5776	2.1533	3.4946	2.271	1.5856	1.407	2.1034	1.503	1.564	1.7047	0.773	1.616	3.4817	1.3744	0.158	
270005M05	ubiquitination	CUL4B	Mm.26885	Hs.155976	0.8748	1.4151	1.302	1.1242	2.8547	1.7677	1.64	1.3472	0.5969	0.9733	1.0466	1.209	0.956	1.879	1.7664	1.331	1.848	1.9114	1.512	1.444	1.2521	0.5808	0.093	
NM_003900	ubiquitination	SQSTM1	Mm.40828	Hs.182248	3.2329	4.1547	2.828	3.528	3.3144	2.2444	2.209	2.051	3.5472	2.0972	5.2052	5.621	5.2139	3.519	4.2638	3.782	4.461	5.016	4.714	6.517	7.8087	1.3975	0.868	
1110001N06	WD40	FLJ1294-v	Mm.277705	Hs.107000	0.8815	0.726	0.36	0.5672	0.9199	1.243	0.677	1.1477	2.0781	2.7419	4.6086	1.305	1.1106	1.257	1.226	1.573	1.017	1.3948	1.44	1.23	1.0722	1.0358	2.157	
1200006M05	WD40	PC326	Mm.219241	Hs.280168	3.5753	1.7933	2.455	1.4341	1.4562	2.2556	0.921	1.096	4.5221	5.6529	6.4171	2.576	2.5117	2.509	3.4548	2.263	3.955	4.0539	4.144	2.974	2.708	0.9437	0.681	
1300004C11	WD40	GTF3C2	Mm.271923	Hs.75782	2.0094	1.2278	1.77	0.6947	1.0683	1.993	0.993	1.1174	1.6719	1.728	1.8538	1.462	1.5707	1.5	1.243	1.991	1.241	1.8749	1.271	1.656	2.1619	0.7096	0.849	
1310001E19	WD40	PPBP2R2D	Mm.258739	Hs.380372	4.6581	4.6697	4.19	5.9445	1.637	1.7979	0.78	1.7131	2.4913	1.734	2.1244	2.342	2.3504	1.562	1.4747	2.074	1.544	1.6895	2.493	2.921	4.5107	1.1093	0.761	
1500001L20	WD40	KIAA1892	Mm.28891	Hs.102669	1.9108	1.3121	1.54	0.6838	0.887	2.5486	1.063	0.3761	4.1266	8.8632	5.3814	1.54	1.4728	1.679	2.6271	2.841	2.672	3.8236	3.398	1.092	1.4997	0.5023	0.846	
150009K01	WD40	APG16L	Mm.272972	Hs.419213	1.0309	0.8393	0.527	0.2084	0.8183	1.6373	1.092	0.9638	2.4823	3.7738	3.0655	1.074	1.0501	1.341	1.7676	2.15	1.52	1.9766	3.083	0.976	0.8788	0.3735	1.004	
1600015H11	WD40	PRPF4	Mm.22833	Hs.374973	1.4367	1.4828	0.793	0.63	0.9044	1.1666	1.51	1.1501	2.3415	3.2143	3.2553	1.419	1.546	1.2921	1.998	1.554	2.3297	2.456	1.839	1.5822	0.5677	0.825		
1700012F10	WD40	HAN11	Mm.9671	Hs.410598	2.5618	2.0558	1.917	1.046	1.8148	1.0607	1.395	1.271	1.4419	2.4041	2.0915	1.045	2.2272	1.666	1.2498	1.271	3.01	3.194	2.6761	1.882	2.678	2.1232	1.118	0.756
170005K18	WD40	CSTF1	Mm.26944	Hs.172865	1.2492	1.4363	1.039	0.8639	0.6778	1.35	0.607	0.8103	0.8662	0.7243	0.84	0.836	0.9373	1.114	0.517	0.817	0.951	0.6267	0.358	1.208	1.3141	0.6318	0.85	
1700120F24	WD40	WDFY1	Mm.293273	Hs.44743	1.8373	2.7309	1.086	0.378	1.3815	1.3543	0.821	0.7038	1.1442	1.1424	0.9269	1.848	1.7365	1.268	1.1083	1.218	1.21	1.2415	0.926	1.294	1.7415	1.1609	0.97	
2310011G05	WD40	FLJ1294-v	Mm.277705	Hs.107000	1.219	1.0163	0.696	0.6025	0.642	0.9825	0.661	0.6772	3.2971	5.5926	3.7499	1.039	1.3055	1.655	1.931	2.021	1.461	2.1358	1.596	1.369	1.6854	0.732	0.966	
2310012I10	WD40	WDR18	Mm.35828	Hs.325321	1.0674	1.2452	1.541	0.5536	1.0493	1.2495	0.684	0.4728	1.6483	2.1871	1.4247	1.235	1.293	1.711	1.8795	1.922	1.474	1.8563	1.658	1.91	1.08	0.4034	0.745	
2310042N09	WD40	CDC20	Mm.289747	Hs.82906	1.6187	1.9874	1.443	0.7812	0.8227	1.4476	0.638	2.5955	3.3618	3.6368	1.591	1.8627	1.229	1.3425	1.766	1.839	1.9139	2.122	1.608	1.6532	0.4507	0.772		
2410003J24	WD40	KATNB1	Mm.25832	Hs.275675	1.5295	1.4889	1.492	0.5882	0.7216	1.2951	0.439	0.884	2.0384	3.4928	3.958	1.866	1.6152	1.798	2.4274	2.09	1.57	1.7826	2.255	1.786	1.6209	0.6001	0.599	
241003L322	WD40	Nup37	Mm.22184	Hs.5152	1.5364	1.0708	1.515	0.5585	1.0025	1.2024	0.948	0.1069	4.619	1.9155	1.2023	0.271	1.062	1.244	0.916	1.05	1.8415	1.257	1.641	1.441	1.496	0.9411	0.83	
2410022P04	WD40	CKN1	Mm.212208	Hs.32967	1.111	0.9487	0.83	0.451	0.8043	1.593	0.759	0.5611	1.0442	1.062	1.2248	0.914	1.1659	1.023	0.73	1.007	1.168	0.929	0.89	0.941	1.1509	0.4027	0.812	
0610007C05	WD40	ARPC1B	Mm.30010	Hs.433500	2.288	2.129	1.35	1.048	0.9542	1.5922	0.495	0.6047	1.0497	1.2336	1.1016	1.364	1.3645	1.048	1.7431	0.901	1.012	1.9282	1.046	2.362	2.5571	0.521	0.675	
483343H09	WD40	GNB3	Mm.130145	Hs.71642	2.1907	1.8032	1.415	0.7229	1.5729	1.5729	0.781	0.4886	3.2932	3.1449	3.6533	2.163	1.6259	1.566	1.9829	1.737	2.449	1.994	2.14	1.754	1.5603	0.7401	0.667	
4930447M07	WD40	WDR20	Mm.219475	Hs.55209	1.8798	1.6562	0.875	0.8241	0.9846	1.9065	0.357	0.5756	6.0653	2.524	2.2967	1.963	2.6633	1.218	1.1442	0.937	1.802	1.6539	1.71	1.778	1.6886	0.7769	0.665	
260017H24	WD40	CHAF1B	Mm.274222	Hs.7528	2.2725	1.6633	1.33	0.8549	0.6544	0.9866	0.422	0.647	1.0335	1.0788	1.3542	1.866	1.661	0.995	1.0537	0.858	1.348	1.0781	1.508	1.998	1.9091	0.7993	0.456	
2700038M07	WD40	WSB1	Mm.287354	Hs.315793	2.2744	1.2979	1.89	1.1148	1.2431	1.7121	1.046	1.0594	3.782	4.4404	4.2667	3.082	2.7926	1.911	2.3964	2.161	1.442	2.444	1.997	2.215	2.3186	1.2219	0.92	0.665
0610009C03	WD40	HRPPB9P	Mm.29606	Hs.379357	0.8327	0.9987	0.964	0.4611	0.4756	0.766	0.571	0.5708	1.7762	1.1956	0.7711	0.895	0.6453	0.964	0.6215	0.97	1.035	1.2305	0.992	1.624	1.0677	0.201	0.916	
2610044M17	WD40	SMU-1	Mm.289929	Hs.327749	1.1556	0.8966	0.947	0.3825	0.9029	1.4207	0.612	0.9179	0.7771	1.0286	0.7017	0.912	0.9187	1.111	0.702	1.196	1.142	1.2152	1.18	2.032	1.365	0.7955	0.564	
493053L09	WD40	PLRG1	Mm.286349	Hs.249996	1.7397	1.6274	1.368	0.6665	0.8755	1.2477	0.673	0.9711	1.3852	1.8078	1.8878	1.445	1.3526	1.173	0.951	1.0544	1.257	1.627	1.4821					

Table S2

4933428O03	kinase	EIF2AK4	Mm.26931	Hs.412102	2.2756	2.4273	1.486	1.8317	3.3582	1.5348	1.354	0.9336	2.5127	5.8244	2.6644	4.192	4.2258	1.319	2.447	1.252	2.01	2.5262	2.947	2.967	2.9543	2.0367	0.472	
1110062I02	kinase	DAPK2	Mm.41755	Hs.129208	1.4193	2.8666	0.889	1.7136	2.0205	1.1595	0.859	0.5515	3.6278	3.6882	3.3594	1.882	2.4751	1.297	1.6409	1.192	1.606	1.7733	1.029	1.913	1.9594	2.6455	0.395	
1200006A05	kinase	CSNK1D	Mm.216227	Hs.378918	1.8171	1.7865	0.774	1.3386	2.4737	0.9721	0.573	0.5611	2.7296	3.2147	1.5042	1.328	1.4467	0.96	1.6166	1.172	1.628	2.1248	0.97	2.786	2.3443	1.451	0.305	
1200013B22	kinase	SNARK	Mm.100666	Hs.17202	3.8309	4.619	1.436	2.5598	3.6804	1.7443	1.036	0.8635	2.5553	5.8749	3.2417	1.543	2.4243	2.0501	3.0161	2.466	1.79	2.533	1.214	2.71	2.5919	1.6489	0.395	
1700014N07	kinase	STK22C	Mm.143802	Hs.512763	2.458	2.3292	1.317	1.6553	5.2373	1.5202	1.24	0.8937	2.0561	2.8363	2.6453	1.513	1.9717	1.632	1.5224	2.491	1.78	2.0011	1.372	2.041	2.9459	1.6409	1.65	
1700029P02	kinase	STK22D	Mm.18470	Hs.333138	2.0432	2.3352	1.239	1.5455	2.2302	1.5135	0.571	0.5103	2.8724	5.5517	2.5546	1.521	2.2795	1.34	2.1028	1.755	2.453	2.4711	2.521	2	2.9266	0.9474	0.316	
2810003O05	kinase	FANCL	Mm.18875	Hs.411433	1.2753	2.0261	0.88	1.1389	2.2212	0.7292	0.757	0.9433	5.9173	8.7878	5.3951	1.444	1.6812	1.697	3.6563	1.814	3.812	2.8539	2.803	2.65	2.521	1.6209	0.443	
2810434B10	kinase	TOPK	Mm.24337	Hs.104741	0.9979	1.3909	0.988	0.8173	3.0066	1.242	2.221	0.3701	0.8459	1.5801	1.0171	1.584	1.3825	1.075	0.8381	0.981	0.988	1.3101	1.169	1.548	1.3482	1.8575	0.703	
2810454O04	kinase	KIS	Mm.209150	Hs.127310	3.8864	4.0706	0.954	2.2375	3.8891	2.221	1.484	1.5516	3.2984	7.2189	3.2126	2.524	3.8419	1.498	3.4908	1.742	2.48	2.3898	3.418	4.081	4.9111	0.902	0.426	
2210022N24	kinase	OSR1	Mm.293565	Hs.95220	2.2283	1.7593	1.407	1.7388	2.9887	1.4874	0.841	0.8743	2.5688	5.1179	2.7623	1.812	2.7074	1.304	2.9655	2.448	3.475	3.3993	2.419	3.459	3.4553	1.6141	0.379	
2810011D23	kinase	CAMK2D	Mm.255822	Hs.111460	1.5669	1.8271	0.811	0.7436	5.1461	1.3554	1.329	1.5539	0.8201	1.8214	1.4466	1.026	1.1599	1.277	0.9794	1.547	0.917	1.1543	1.277	2.085	1.8447	1.7815	0.635	
4632401F23	kinase	NEK8	Mm.23788	Hs.448468	2.2038	1.8322	1.098	1.2596	2.3801	0.9319	0.405	0.7377	3.0975	5.0944	3.2187	1.909	2.5984	2.306	4.24	2.546	2.707	2.2552	2.452	2.38	2.6777	0.6001	0.435	
4632404G05	kinase	CSNK1A1	Mm.26908	Hs.318381	1.8393	1.4434	0.777	0.8842	2.4786	1.1369	1.65	1.4766	2.9433	7.355	1.9101	1.226	1.5266	1.558	1.7139	2.204	1.269	1.2779	1.528	1.447	2.1541	0.9119	0.593	
4833246L05	kinase	HRI	Mm.220921	Hs.434986	1.2392	1.2191	0.621	0.809	1.6355	1.5598	0.951	1.1561	2.6892	4.6564	2.6339	1.279	1.2943	1.384	2.1024	1.957	1.362	1.4744	1.221	1.882	1.786	1.8201	0.826	
4921505G21	kinase	STK33	Mm.79075	Hs.148135	0.6238	1.3999	1.15	0.8478	1.8437	1.2032	1.162	1.3484	0.4382	1.7832	0.5776	1.58	1.2308	1.176	0.9217	0.936	0.875	1.1297	1.013	1.886	1.4887	1.9266	0.696	
4921506N09	kinase	TLK2	Mm.126976	Hs.445078	0.8743	1.3057	1.373	1.0106	2.529	1.9101	1.022	1.0462	1.7671	2.8774	2.0892	1.674	1.49	1.261	0.8301	1.103	1.479	1.4625	0.763	1.673	1.9336	1.1124	0.453	
4930444A02	kinase	FLJ23356	Mm.17631	Hs.277431	0.8264	1.0823	0.722	0.6849	1.5867	0.8451	0.255	0.4402	12.598	11.57	10.79	1.197	1.3698	1.356	1.6841	1.413	10.457	3.5983	8.571	1.634	1.3959	0.8074	0.09	
4930588B12	kinase	PFTK1	Mm.6456	Hs.57856	2.1061	2.1618	1.145	1.5229	2.3094	1.2409	1.31	1.2432	3.7863	8.3266	3.7179	1.318	1.6767	2.366	3.5831	2.311	2.479	3.1181	1.821	2.623	3.1806	1.7386	0.511	
4930594I21	kinase	STK22C	Mm.143802	Hs.512763	1.9673	2.4672	1.535	1.4258	4.925	2.3338	1.074	1.2746	1.7209	2.8779	2.8112	1.414	1.9127	1.908	1.5853	2.086	1.421	1.8284	1.736	1.41	2.559	1.3906	0.545	
5730422C08	kinase	PAK1	Mm.260227	Hs.64056	2.3372	3.0302	1.243	1.7136	3.3069	2.4976	0.98	1.4173	10.836	12.065	9.4093	1.67	3.3437	1.627	2.986	2.933	3.2206	4.234	5.722	5.8177	1.0831	0.304		
6330415L08	kinase	IRAK2	Mm.152142	Hs.424542	2.2778	3.7253	1.019	1.5989	1.647	1.4253	0.286	0.3749	1.4184	1.3806	1.0913	1.26	1.7544	1.974	1.158	0.868	1.491	5.5372	0.7737	0.197				
6430598J10	kinase	PCTK2	Mm.45746	Hs.258533	1.0064	1.4401	0.802	1.1156	1.1898	0.7643	1.243	0.4293	1.6824	4.8157	1.6395	1.177	1.183	1.286	1.6455	1.647	1.137	1.6607	0.719	1.923	2.2341	1.4977	0.584	
9030416P08	kinase	MYO3A	Mm.221230	Hs.148228	0.7312	2.317	0.984	0.8602	1.6231	1.4518	1.432	1.4512	2.2164	7.4585	2.795	1.985	1.3444	1.875	2.0405	1.571	1.931	2.7599	1.248	1.73	1.3353	1.6682	0.801	
9130411F08	kinase	CHUK	Mm.3396	Hs.198998	0.6944	2.1322	1.09	1.1874	2.5574	1.7161	0.925	1.1114	1.5395	3.7057	1.6614	1.75	1.4116	1.788	2.3296	1.679	1.904	2.1663	2.246	1.949	2.5133	2.2179	0.678	
9130423C03	kinase	CDK6	Mm.88747	Hs.38481	1.0613	1.0528	0.694	0.6401	1.4044	0.7684	0.467	0.5454	1.8215	2.4041	1.1446	1.248	1.3205	0.887	1.3731	1.064	1.475	1.5641	1.829	0.903	1.4062	0.744	0.292	
4432415E19	kinase	MAP4K5	Mm.291936	Hs.246970	0.7043	0.5332	0.278	0.2825	0.1449	0.1938	0.348	0.2467	0.4259	0.4142	0.4096	0.0448	0.8985	0.603	0.6115	0.689	0.615	0.509	0.309	1.191	1.1851	1.1808	0.245	
L11695	kinase	TGFBR1	Mm.197552	Hs.2805	1.7641	1.6884	1.31	1.4315	2.518	2.4916	1.035	0.8647	23.13	61.051	10.224	1.473	1.3727	14.18	11.597	11.6	45.91	58.173	41.194	2.881	2.3559	0.7731	0.089	
NM_001204	kinase	BMPR2	Mm.7106	Hs.53250	1.2287	0.9473	0.808	1.1754	1.8422	0.8833	1.494	0.5744	19.085	3.7122	13.399	1.237	1.3018	1.538	1.0032	1.427	1.1	1.5879	16.436	2.288	2.6603	0.6928	0.338	
L29479	kinase	STK18	Mm.3794	Hs.172052	1.3512	1.5709	2.311	1.4003	3.4628	1.7533	1.31	1.8731	2.8171	1.8454	1.6498	1.635	1.67	1.446	1.439	1.779	1.645	2.1637	1.7208	1.816	2.576	2.1761	0.186	
D76446	kinase	MAP3K7	Mm.258589	Hs.290341	2.3213	1.7527	1.18	1.3047	0.7162	1.6143	0.472	0.2673	2.8249	1.5398	1.8455	1.817	1.3481	1.9761	1.276	1.244	1.0891	1.541	5.075	4.2593	0.7227	0.334		
1200014P03	TPR	KNSL8	Mm.279599	Hs.53447	2.2289	2.2929	1.212	1.6116	1.5294	1.9153	0.687	0.5031	1.3984	2.8028	7.1136	3.41	1.143	0.6168	1.6148	1.7545	1.078	1.064	1.211	1.757	2.4243	1.6981	0.818	
4933404O19	TPR	DCKFZ434H	Mm.31590	Hs.201134	1.0581	0.6475	0.403	0.3897	0.4906	0.9898	0.788	0.8635	0.6340	0.6464	0.6717	0.8444	1.194	0.965	1.081	1.6010	0.747	0.876	0.7656	0.653	1.726	1.236	0.8914	0.737
4930506L13	TPR	PEX5R	Mm.151332	Hs.46780	1.1274	0.926	0.728	0.5104	1.2889	0.8173	1.171	0.3568	1.127	1.5378	1.555	1.325	0.6729	1.12	1.3081	1.167	1.244	1.722	1.251	1.1857	1.8475	0.617		
4930564J03	TPR	APPBP2	Mm.271997	Hs.84084	0.6139	0.8807	0.525	0.3675	0.3252	0.7505	0.578	0.7135	1.4341	0.995	0.9248	0.913	1.006	1.396	1.3876	1.148	1.0286	1.056	1.755	1.775	2.0226	1.4709	0.809	
2210019E14	TPR	MGC29649	Mm.259531	Hs.31704	2.1493	1.6082	0.979	0.7067	1.3805	1.7043	1.51	1.1634	1.1104	2.0952	1.6295	0.998	1.4183	1.081	1.2867	1.574	1.272	0.9713	2.016	1.671	2.4075	1.3458	0.201	
201003F24	TPR	DNAJC7	Mm.258140	Hs.446481	1.1155	1.0129	0.498	0.4799	0.3128	0.057	0.387	0.2394	1.4707	2.0213	2.1001	1.087	1.667	0.871	1.3298	0.832	1.007	0.9067	1.235	1.006	3.4669	0.6947	0.339	
290001004	TPR	OSRF	Mm.259479	Hs.280																								

Table S2

4930429H24	BTB/POZ	DRE1	Mm.274579	Hs.246875	1.2687	0.97	0.731	0.3882	0.6798	1.1961	0.577	0.7014	1.9317	1.9703	1.3626	1.853	0.7633	1.098	1.4198	1.536	1.733	1.7733	1.944	2.25	1.757	1.1391	0.551	
1200003E21	BTB/POZ	LZTR1	Mm.161726	Hs.78788	1.9808	1.6346	1.971	0.4762	1.5608	2.7064	0.849	0.8453	2.0604	1.3835	2.4025	1.513	0.9717	1.589	1.035	1.592	3.229	2.7074	3.04	2.178	1.4604	0.8379	0.745	
1300017A20	BTB/POZ	ZNF288	Mm.211212	Hs.436987	0.7607	1.0755	0.687	0.1888	0.4243	0.7335	0.43	0.5478	0.706	0.6333	0.5125	1.297	0.6147	0.159	0.6339	0.779	0.798	0.7334	0.682	1.1	0.9517	0.3592	0.243	
2610021A10	PH	SCAP2	Mm.156651	Hs.401745	1.8456	0.9339	1.765	0.6443	1.0608	1.8766	1.43	1.161	1.9809	5.6707	2.515	1.509	1.1001	1.707	2.6553	1.796	1.643	2.1527	1.26	1.423	1.539	0.7451	1.071	
6430512N22	PH	PLEKHA2	Mm.261122	Hs.470847	2.3587	2.0895	0.893	1.7343	1.77	1.5091	0.591	0.6966	1.5128	2.4596	1.3517	1.788	2.4109	0.907	0.9365	1.018	1.632	1.1441	1.716	2.653	2.501	0.7775	1.038	
A430106A18	PH	ITK	Mm.274218	Hs.211572	1.2876	1.0095	0.9	0.7684	1.0832	3.0508	0.316	0.2975	2.7219	3.8575	2.5745	1.183	2.322	1.281	1.1682	1.671	1.674	1.0687	1.775	1.419	1.3327	0.6717	0.978	
4933426D16	PH	SNTG1	Mm.129083	Hs.388360	1.9986	0.9861	0.896	0.7161	1.7496	2.7147	1.317	1.1706	4.1048	5.5779	4.9218	1.863	2.8396	1.946	1.9667	2.399	2.613	2.1671	1.413	1.445	1.9768	0.5665	1.09	
5730427K19	PH	APS	Mm.277333	Hs.371366	1.0663	0.9801	1.086	0.586	1.4592	1.322	1.331	1.5806	1.266	2.6388	1.2942	1.222	1.6371	1.183	0.8691	1.18	1.321	1.0357	1.206	0.836	0.9639	0.6916	1.2	
1810074L23	PH	PLEK	Mm.98232	Hs.77436	1.632	1.1046	0.395	0.8466	1.3282	1.124	0.808	1.4319	2.1677	4.8873	1.5378	1.9	0.3899	4.839	1.6255	2.005	1.556	2.2628	2.331	1.653	1.1644	0.7961	1.366	
2010320F03	PH	PLEK2	Mm.103380	Hs.170473	1.2745	0.9767	0.311	0.6879	0.3685	0.5558	0.695	0.4499	0.6707	0.8728	1.2597	1.38	1.1173	1.31	0.7321	0.922	0.799	0.6707	0.813	1.705	1.149	0.5409	0.605	
150001N23	PH	PLEKHBT1	Mm.26633	Hs.445489	2.992	2.0725	1.442	2.0622	2.139	2.276	1.005	0.4692	14.249	11.15	9.5328	3.467	3.8001	3.156	6.6784	3.765	11.272	7.2872	5.948	2.794	2.873	0.9511	1.218	
1200014M06	PH	OSBPL3	Mm.44153	Hs.197955	2.6369	2.1386	0.877	2.2149	1.6201	2.4574	0.611	0.7498	2.1054	2.5798	1.357	2.322	3.0502	1.616	1.5437	1.168	1.275	2.0164	2.78	4.503	3.7963	1.1883	1.426	
1200004I20	PH	ARHGEF3	Mm.207446	Hs.25951	1.5991	1.4124	0.818	1.1156	0.9438	1.0137	1.377	0.3821	1.3382	1.3544	0.8035	1.858	2.7978	1.174	0.9597	1.05	1.404	0.8206	1.293	2.831	2.9324	0.4132	2.124	
3110056A02	PH	POLR2J2	Mm.127418	Hs.406505	2.2235	1.4971	0.824	1.6997	1.6126	2.2556	1.091	1.3073	2.33	3.1546	2.0474	2.207	4.2265	2.27	2.4474	2.394	2.77	2.3737	2.12	2.489	2.5971	0.1656	1.916	
4933433D06	PH	OSBPL10	Mm.259777	Hs.368238	1.447	1.361	0.612	0.8662	0.6136	0.6931	0.558	0.6651	1.3501	1.49	1.098	1.012	2.2839	0.868	1.04	1.379	0.5344	1.063	1.579	1.5236	0.2154	0.682		
2410043H07	PH	PSCD2	Mm.272130	Hs.8517	0.884	1.1554	0.452	0.6669	0.4452	0.6499	0.414	0.2975	0.7734	0.8897	0.8483	0.946	0.9261	0.947	0.7895	0.916	0.809	0.5098	1.148	1.047	1.1058	0.3393	1.357	
2810471M23	PH	FLJ12604	Mm.235383	Hs.126485	2.6924	2.2585	1.624	2.315	1.0329	2.0744	0.849	0.7498	14.969	12.47	10.012	4.559	0.171	6.022	3.7771	3.512	2.163	2.9742	3.465	2.038	2.5223	0.8428	1.189	
9530063M10	PH	GNRPX	Mm.41479	Hs.512626	1.7741	1.4398	0.783	1.4285	1.0259	1.3271	0.617	0.7607	3.724	3.575	2.895	2.225	1.9785	3.458	2.511	1.82	1.933	1.7056	1.388	1.642	1.4746	0.0616	0.94	
6230420N16	PH	FLJ12987	Mm.255342	Hs.296730	1.7079	1.0222	1.058	0.9512	0.766	1.7549	0.625	0.7933	1.852	3.6644	1.8731	1.496	1.7708	1.37	1.5777	1.316	1.296	1.3592	1.269	1.422	1.3198	1.0265	1.016	
5031433E13	PH	SWAP70	Mm.282528	Hs.153023	1.021	0.969	0.502	0.7936	1.0244	1.0392	1.273	0.624	1.6295	2.8425	1.5795	1.345	3.1048	1.366	1.2836	1.141	0.936	0.5699	0.728	1.549	1.9949	0.7146	1.341	
4933427A08	PH	FGD6	Mm.269596	Hs.170623	1.6154	1.143	0.394	0.8903	0.7914	1.3503	1.028	0.9397	1.3435	2.0552	1.0807	1.52	1.9598	1.508	3.109	2.236	1.185	1.08054	0.856	1.488	2.4024	0.7812	1.312	
9130014M22	PH	FLJ10244	Mm.28376	Hs.220745	2.5345	2.1411	0.527	1.6229	1.1161	1.7071	0.728	0.6107	5.6313	10.26	5.0977	2.281	3.6238	1.481	2.9901	2.771	3.99	2.9979	4.006	4.269	4.3624	0.8634	1.066	
5830480G12	PH	ARHGAP15	Mm.239239	Hs.433597	0.758	1.0508	0.796	0.7048	0.7231	0.9973	0.935	1.0243	2.743	4.3762	3.1181	1.405	1.7507	1.14	1.2628	1.305	1.603	1.0857	0.929	3.843	3.2341	1.4043	2.07	
2810487K12	PH	PSCD3	Mm.281003	Hs.7984	0.8342	1.013	0.21	0.8463	0.4104	0.5722	0.149	0.1657	0.6748	0.5387	0.642	0.829	1.0516	0.687	0.6656	0.664	0.567	0.3133	0.424	1.568	1.3121	0.7619	0.46	
2410008H17	PH	GEFT	Mm.22583	Hs.61581	2.231	2.0019	1.055	1.3014	0.8023	1.296	0.493	0.5563	2.543	2.9282	2.3555	2.123	3.5693	1.275	1.224	1.215	2.485	1.5718	1.31	1.457	1.8769	0.0419	1.07	
2810052M02	PH	CKIP-1	Mm.29475	Hs.173380	1.4572	1.6615	0.976	1.7903	0.4721	0.6007	0.213	0.335	0.7387	0.5338	0.3805	1.79	1.965	1.595	0.6203	1.222	0.731	0.708	0.53	6.305	3.6674	1.7672	0.476	
1700038J09	PH	ARHGEF5	Mm.261443	Hs.372802	3.0382	1.7584	1.866	3.0194	1.9209	2.6425	0.971	0.8731	0.3782	4.0595	2.5032	0.944	3.8785	1.748	2.0952	1.56	2.252	1.7598	3.261	2.313	2.5036	0.9424	0.481	
1300015B16	PH	DM2	Mm.39292	Hs.438225	0.8051	0.6946	0.664	0.4464	0.4672	0.5821	0.276	0.289	0.5698	0.4477	0.4739	0.9	0.826	0.703	0.4666	0.69	0.689	0.3862	0.777	1.361	1.2173	0.4108	0.545	
0610010K16	PH	RGS19P1	Mm.20945	Hs.6454	0.7166	0.5897	0.966	0.4716	0.3885	0.5176	0.853	0.7183	0.871	0.875	0.3725	1.46	0.13	1.949	0.6874	1.165	0.909	1.1382	1.14	1.227	1.0858	0.6586	1.124	
2610024J09	PH	AUP1	Mm.275961	Hs.411480	1.0753	0.7668	0.682	0.7737	0.7231	0.9973	1.161	1.0703	1.050	1.050	1.050	1.050	1.050	1.050	1.050	1.050	1.050	1.050	1.050	1.050	1.050	1.050		
2700099C19	PHD	LOC51248	Mm.291607	Hs.11042	1.2674	1.1607	0.946	1.2647	1.1607	1.2647	0.946	1.2647	1.2647	1.2647	1.2647	1.2647	1.2647	1.2647	1.2647	1.2647	1.2647	1.2647	1.2647	1.2647	1.2647	1.2647		
4833411E15	PHD	SDCBP	Mm.247473	Hs.164067	0.9446	1.0552	1.0552	0.9446	0.9446	0.9446	0.9446	0.9446	0.9446	0.9446	0.9446	0.9446	0.9446	0.9446	0.9446	0.9446	0.9446	0.9446	0.9446	0.9446	0.9446	0.9446		
4921513F16	PHD	PDK1	Mm.5271	Hs.178170	2.203	1.4991	1.08	0.6638	1.9483	2.2717	1.053	0.5841	5.7725	5.8433	4.6749	2.135	1.2903	3.158	3.6084	4.271	2.788	2.7574	2.385	3.362	2.9414	0.8366	0.747	
1700094E07	phosphatase	STYX	Mm.202561	Hs.364984	0.9855	0.9601	0.419	0.3031	1.4781	2.0406	0.72	0.9904	1.2588	0.6267	1.222	1.871	1.6041	0.871	0.916	1.05	1.073	1.2085	1.104	1.564	1.3701	0.7961	0.842	
1300019I03	phosphatase	DUSP6	Mm.1791	Hs.298654	1.2614	1.0895	1.368	0.472	2.2112	1.174	0.584	0.9348	1.3744	6.112	1.1527	2.299	1.071	2.322	1.9859	1.267	1.3694	0.76	0.492	0.9974	0.7856	1.283		
1190004O14	phosphatase	DUSP12	Mm.34365	Hs.416216	1.2857	1.2125	1.234	1.294	0.2968	1.0399	1.0544	0.621	0.8175	0.84	0.9429	0.6733	1.981	0.7177	1.3	0.8025	1.257	0.937	1.0298	0.778	1.469	1.0045	0.7538	0.487
1600009009	phosphatase	ILKAP	Mm.234179	Hs.92033																								

Table S2

2410002J21	LIM	ENIGMA	Mm.275648	Hs.436339	1.1329	1.4843	0.773	1.067	0.6509	1.3619	0.611	0.9046	0.7669	0.9688	0.5649	1.042	1.5923	0.879	0.7181	0.82	0.867	0.4861	0.565	1.329	1.3746	1.0638	1.408
4931439A04	zf-C3HC4	DKFZp434J1	Mm.120835	Hs.104744	1.4679	1.3543	1.075	1.3732	3.044	1.1388	1.215	1.3738	1.7353	2.5797	2.1668	1.901	1.6551	1.267	2.281	1.384	1.614	1.8563	1.023	2.608	2.8569	1.2761	0.245
A430106H13	zf-C3HC4	TRIM35	Mm.288225	Hs.137732	3.4469	5.2823	1.49	3.9605	6.6547	1.7792	1.287	0.9735	1.877	2.1769	1.0484	8.776	6.3977	1.173	0.9083	1.268	1.377	1.7327	0.985	2.968	3.9246	1.7902	0.632
2610509H23	zf-C3HC4	RNF146	Mm.28930	Hs.267120	1.6831	2.1448	0.381	1.4601	2.8278	0.9813	1.532	1.3895	0.8092	1.5551	3.7221	1.857	1.5774	1.473	0.9284	0.849	1.17	1.2508	1.024	2.312	1.973	2.1034	0.409
2610005D23	zf-C3HC4	RNF14	Mm.22086	Hs.170926	2.4877	2.7656	1.998	2.7193	3.0534	1.4354	1.716	1.3496	2.2379	2.6876	2.3805	3.284	2.9128	1.582	1.0828	1.479	1.797	1.9029	0.691	4.186	4.4334	3.6965	1.062
2700043E10	zf-C3HC4	RNF2	Mm.31512	Hs.124186	1.9027	1.8015	1.445	1.7038	2.5873	2.4794	1.724	1.7269	2.2669	2.5759	1.9032	1.844	2.3497	1.108	1.9727	1.473	1.667	1.366	0.83	2.34	2.6022	4.6219	0.768
2310043C01	zf-C3HC4	TRIM34	Mm.25466	Hs.125300	0.9912	1.4933	1.347	0.7556	1.6933	0.9935	1.196	1.2238	0.9831	1.0883	1.196	1.018	0.9978	1.38	1.2992	1.054	1.627	1.0975	1.403	1.514	1.6138	1.0146	0.083
2510042A13	zf-C3HC4	Rnf130	Mm.166372	Hs.526059	0.6031	0.9228	0.317	0.7646	0.9806	1.1149	0.736	0.8151	10.742	9.6882	15.269	1.57	1.1472	1.2	2.3153	0.914	1.661	1.4016	0.966	1.759	2.1341	1.3333	2.583
2610110L04	zf-C3HC4	RNF141	Mm.268926	Hs.44685	1.7375	1.7233	2.479	1.8242	2.0265	1.0138	1.364	0.9445	1.0159	0.929	0.8657	2.117	2.1375	1.074	1.1596	1.116	1.207	1.0383	1.033	1.891	4.3979	1.1846	0.125
2810430O10	zf-C3HC4	RNF12	Mm.44069	Hs.122121	0.9976	1.1954	0.982	1.1227	1.2635	0.8856	0.577	0.5527	0.781	1.5419	0.8023	1.624	1.3332	1.011	0.9727	0.984	1.058	0.9976	0.54	3.447	4.4153	1.489	0.075
3110001L12	zf-C3HC4	RFP2	Mm.23959	Hs.436922	1.1497	1.3076	0.855	1.2036	2.2949	0.705	1.219	1.2879	1.7621	2.2639	2.6283	1.482	1.3563	1.81	1.5056	1.74	1.824	1.792	0.508	2.399	2.581	1.3309	0.088
2410015A17	zf-C3HC4	RNF138	Mm.253542	Hs.180403	2.2589	2.2679	2.083	2.8141	3.2722	1.6155	0.949	0.8961	2.5791	3.7901	1.3552	3.604	3.2832	1.349	1.5492	1.084	1.354	1.67	0.924	2.829	4.6687	1.357	0.362
1300004G08	zf-C3HC4	FLJ23360	Mm.267353	Hs.161279	2.6688	3.0791	1.757	2.7058	2.525	1.5863	1.351	0.884	2.0694	1.225	1.5796	3.567	3.4102	1.355	1.9847	1.395	1.65	1.2474	1.472	2.466	4.7087	1.2618	0.762
2410131O05	zf-C3HC4	RNF5	Mm.274542	Hs.512071	1.0806	1.2818	0.401	1.0407	2.1236	0.9376	1.343	0.9951	3.4497	2.8825	2.5707	2.179	1.6528	1.669	1.9837	1.655	1.717	1.8953	1.111	2.773	1.512	1.8151	0.72
4921523A11	SH3	NCK2	Mm.144978	Hs.101691	1.2538	1.2473	0.952	0.8666	0.503	0.854	0.694	1.3557	0.8101	1.0467	0.9691	1.355	1.734	0.7609	1.332	1.332	0.8917	0.581	1.58	1.9169	1.0551	1.298	
1200007H22	SH3	SH3KBP1	Mm.167131	Hs.153269	0.8376	0.8339	0.413	0.4284	0.4726	0.3734	1.325	1.473	0.4748	0.694	0.5143	0.99	0.897	1.257	1.4805	0.841	0.669	1.1263	3.001	1.391	0.8014	0.8403	1.131
160023G18	SH3	OSTF1	Mm.172222	Hs.47011	2.0535	0.6592	1.92	0.2858	0.4681	1.8011	0.674	0.8707	0.9954	1.0129	0.5488	0.849	0.9179	1.112	0.8116	1.141	1.02	0.6064	1.298	1.232	0.7041	0.6331	1.172
2610511H05	SH3	SH3GL3	Mm.736	Hs.518629	0.8614	0.6265	0.765	0.2121	0.5528	0.5337	1.28	1.5213	0.9912	1.1521	0.4735	0.749	0.8141	1.102	0.7115	1.107	1.52	1.3283	1.42	1.02	0.9355	0.6107	1.189
4632407K17	SH3	Tmt1-v2	Mm.258670	Hs.411875	2.2081	1.2513	1.981	0.8564	0.9373	1.5263	0.935	1.1731	1.5922	2.0829	1.4758	0.957	1.1016	1.127	1.2023	1.437	1.251	1.1153	1.025	1.547	1.5642	0.6312	1.226
4930572H05	SH3	SRGAP1	Mm.249576	Hs.408259	2.5703	1.6754	1.861	1.4522	1.4981	2.8511	1.69	1.8793	1.3167	2.8024	1.6075	1.839	1.9389	1.904	1.7823	2.311	1.912	3.4188	2.029	1.63	1.5139	0.7912	1.212
6330143E15	SH3	PACSIN3	Mm.288733	Hs.334639	0.5863	0.9153	1.05	0.5284	0.4149	0.5978	0.572	0.5829	0.4199	0.5583	0.4527	1.01	1.077	1.266	0.3478	1.236	0.889	0.8325	0.868	1.382	0.8775	0.8123	1.121
8430435N19	SH3	GRAP	Mm.202760	Hs.176576	0.9317	1.1746	0.632	0.3404	0.2889	0.7923	0.358	0.3314	1.6949	2.0458	1.0645	0.8404	0.9007	1.029	0.8152	1	1.056	0.8968	1.232	0.77	0.5274	0.3922	0.384
2310034C04	SH3	NOXO1	Mm.269293	Hs.191762	1.2631	0.9996	1.073	1.3573	2.1222	1.7361	1.021	1.5322	0.5524	0.4084	3.3248	1.663	0.8686	2.233	2.46	1.827	1.433	1.9622	1.537	1.881	1.6287	0.5785	0.75
1200013B08	SH3	Cxorf9	Mm.276131	Hs.61469	2.3862	2.0524	1.392	1.9851	4.3015	1.3696	2.259	2.3802	1.4511	2.7808	0.953	1.548	1.7917	2.737	2.2227	2.213	1.455	0.9544	3.429	1.485	3.6777	1.4753	0.768
4930548L11	SH3	SAMSN1	Mm.131406	Hs.221851	0.4819	0.9274	0.536	0.6541	2.5106	1.4666	1.112	1.3387	0.9936	2.1918	1.124	1.11	0.8462	1.253	1.2823	1.277	1.159	1.5252	1.015	1.197	1.5145	1.629	0.426
4632411K03	SH3	Tmt1-v1	Mm.258670	Hs.411875	2.7456	3.5469	1.339	2.242	2.9249	1.7813	1.128	1.2758	3.1846	4.3769	3.1907	2.557	4.3556	1.52	1.9105	1.463	2.461	3.1994	2.28	5.986	6.7274	2.0996	0.36
2610016A03	Acetyltransferase	ELPL3	Mm.29719	Hs.267095	1.9791	1.4587	1.097	1.3593	1.1016	0.8726	0.629	0.4765	2.2505	2.1087	2.7772	3.938	2.7395	0.86	1.3021	1.142	2.178	1.6183	1.214	3.352	4.1368	0.7096	0.075
1810018F03	Acetyltransferase	Cmlf1	Mm.46315	Hs.458287	1.345	1.5157	1.054	1.3213	2.3034	2.2037	0.941	1.2396	1.7391	2.5083	1.4755	1.928	1.6177	1.636	2.5319	1.653	1.207	1.9131	1.041	1.87	2.7331	1.1043	0.085
1500004D14	Acetyltransferase	NAT5	Mm.151168	Hs.109253	2.1497	1.7324	1.513	2.1559	1.895	1.1666	0.633	1.3133	3.2328	5.8407	3.3986	3.251	3.0674	2.863	3.8557	2.428	2.641	3.5983	2.094	3.676	4.6042	1.6296	0.082
1200013C24	Acetyltransferase	FLJ14154	Mm.133257	Hs.312841	1.7811	1.5352	1.443	1.3503	2.6879	1.0195	0.437	0.8344	2.0126	2.2128	0.9378	1.619	1.4736	1.39	1.2329	1.446	2.122	1.0653	0.812	2.386	2.2786	1.1678	0.138
1110028N05	Acetyltransferase	DKFZP564C	Mm.86823	Hs.144058	1.4204	2.1388	1.201	2.1281	2.1983	1.6617	1.458	1.2456	1.7384	2.2527	1.045	3.249	2.9495	1.358	1.0583	1.266	1.288	1.6327	0.863	1.511	2.2483	1.7218	0.372
1810043014	Acetyltransferase	GPNP1AT	Mm.233534	Hs.478025	1.1848	0.4147	0.472	0.873	1.1146	2.089	0.811	0.2528	0.9678	2.0003	0.5459	0.977	1.7731	1.357	0.955	1.003	1.146	0.603	1.124	1.138	1.6796	0.6548	0.954
2310011G05	PHD	ING4	Mm.262547	Hs.108183	1.1788	1.142	0.418	0.7695	1.3362	1.5557	0.163	0.6397	0.9869	1.1857	0.7771	1.574	2.1286	0.948	0.8544	1.009	1.167	0.6216	0.648	1.572	1.1657	0.5521	0.975
1200016G04	PHD	DPF2	Mm.259204	Hs.13495	1.1677	1.1945	0.89	0.9516	0.7894	1.0725	0.721	0.7619	1.426	1.9868	1.3841	1.488	1.7544	1.427	1.0652	1.3	0.983	0.7266	0.699	1.446	1.3798	0.7918	0.806
D230038D111	PHD	MLL5	Mm.205190	Hs.380201	0.3964	0.5193	1.051	0.3919	0.4173	1.1749	0.979	1.3339	0.585	1.5844	2.018	1.36	1.0038	1.926	1.6728	1.242	1.076	1.011	1.923	0.7125	0.9175	0.789	
1300012O03	armadillo	AP2B1	Mm.39053	Hs.370123	2.0783	1.2544	0.829	1.008	2.1943	3.1248	1.376	0.9856	1.7688	1.5227	2.009	1.379	1.6177	1.424</									

Table S2

903061B09	SH2	STAT1	Mm.277406	Hs.21486	2.7457	1.9036	1.403	1.9156	3.3846	3.4277	0.702	0.9082	1.9657	2.4531	4.1188	2.15	2.4572	2.46	3.9826	2.039	1.823	2.4534	1.794	1.981	3.1432	2.5441	2.486
A930009E21	SH2	SLA2	Mm.31910	Hs.334489	1.2008	0.9483	0.872	0.4416	0.5887	1.2472	0.611	0.8332	1.1764	1.7593	2.5367	1.395	1.3123	1.202	0.7546	1.197	1.572	1.0958	1.083	1.311	1.4481	3.1298	2.508
4933424C13	SH2	LOC284948	Mm.128597	Hs.209542	1.4768	0.847	1.401	0.2783	1.259	2.2549	0.574	0.5696	1.357	1.4714	0.9988	1.33	0.6244	0.972	1.034	1.23	0.946	0.8545	1.162	2.138	1.6499	0.5366	0.792
2610014F08	SAM	FLJ36175	Mm.288734	Hs.20848	1.0598	0.9558	0.977	0.2753	0.8945	1.2603	0.536	0.4813	0.8419	1.0664	0.8466	1.405	0.7685	1.064	0.6321	0.892	1.057	0.8723	0.547	1.866	1.7254	0.5845	0.578
1110008G13	SAM	PPFA14	Mm.295105	Hs.153648	1.3261	1.0864	1.75	0.4024	0.9154	1.0998	0.453	0.5297	1.898	2.3084	2.1523	1.852	1.0516	1.658	1.8023	1.786	1.539	1.0306	2.055	2.579	1.7408	0.7308	0.682
2010107E08	SAM	EPHA1	Mm.250517	Hs.89839	0.7362	0.491	0.169	0.4886	0.4896	0.6277	1.581	1.4512	0.8707	1.6178	1.406	1.233	0.8455	1.029	0.6837	0.87	1.013	1.2754	1.787	1.127	0.6183	3.0165	0.49
8030473B06	SAM	ETV6	Mm.269995	Hs.171262	1.187	1.2172	0.521	1.0512	1.5524	0.9532	1.367	1.6157	1.1432	1.9007	0.9809	1.789	1.2846	1.176	0.7345	0.927	1.2	1.3829	1.565	3.397	1.5919	2.2671	0.418
1700021J16	SAM	SAMD8	Mm.236484	Hs.282105	0.6584	0.9256	0.419	0.6582	0.763	0.6811	0.392	0.3568	3.6981	3.9092	2.5632	1.099	0.9747	0.906	1.3958	2.009	2.742	1.5235	1.383	1.641	1.354	1.07	0.189
2610002F09	FKBP	FKBP4	Mm.12758	Hs.848	0.7793	1.6788	1.078	1.5063	1.4064	1.1394	0.829	0.5164	0.7408	1.8164	1.341	1.149	1.6932	3.822	1.33	1.782	1.158	1.8648	2.255	1.35	1.078	0.6337	9.184
2700038N19	FKBP	FKBP3	Mm.28480	Hs.379557	1.3414	0.8542	0.578	0.5743	0.5883	0.7097	0.49	0.722	0.4503	0.6498	0.5816	1.098	0.9948	0.809	0.6047	0.912	0.893	0.719	0.356	1.453	1.7357	1.8531	1.503
1110002023	FKBP	FKBP11	Mm.30729	Hs.43869	0.8391	0.8744	0.528	0.7255	0.4532	0.3788	0.28	0.3229	3.3366	1.2497	1.6716	1.443	1.1502	1.281	0.7153	1.177	2.355	1.7217	1.616	1.426	1.0452	0.9206	1.277
1500011D07	FKBP	FKBP1B	Mm.20453	Hs.407482	1.0642	0.6711	0.278	0.5627	0.3192	0.5555	0.617	0.5744	86.518	45.981	113.18	1.508	1.2062	2.484	1.4554	1.081	16.365	13.258	4.293	1.155	1.0148	1.4647	1.887
0610037L19	FKBP	FKBP1A	Mm.278458	Hs.37463	1.139	0.8072	0.965	0.4622	0.4502	0.6223	0.551	0.7087	46.276	19.842	77.171	1.336	1.0307	1.837	1.2498	1.88	4.206	6.1736	1.954	1.427	0.9343	0.9138	1.636
NM_004799	Miscellaneous	MADHIP	Mm.150197	Hs.162051	2.3762	0.7408	0.972	1.2246	0.5568	1.2246	0.939	1.2238	0.4227	0.6367	0.7605	1.255	0.8798	1.066	1.1038	1.017	1.613	1.0433	1.66	1.075	0.8182	0.8721	0.615
AF0693303	Miscellaneous	FOXH1	Mm.42011	Hs.159251	1.5626	0.8444	0.473	0.689	0.7102	1.4087	0.792	0.7268	0.4181	1.3599	0.6771	0.923	0.8977	1.136	0.8173	1.015	1.64	0.8096	0.283	1.241	1.2766	0.8161	2.782
Y13149	Miscellaneous	GSC	Mm.129	Hs.440438	4.9539	3.1626	2.639	8.4761	0.5369	0.6337	0.489	0.5793	1.0575	1.8405	3.446	2.1054	1.336	1.5603	1.84	1.366	1.5218	1.238	1.089	1.6983	1.3284	1.463	
0610039E12	Miscellaneous	IRF7	Mm.3233	Hs.166120	2.892	2.26	1.075	2.1627	1.7844	2.1747	0.344	0.8103	2.3472	0.3048	3.1604	2.53	2.4258	1.541	1.9559	2.124	3.477	2.4449	3.377	1.588	1.7221	1.817	1.64
311001G18	Miscellaneous	IRF3	Mm.3960	Hs.75254	0.3222	1.1534	0.908	0.9798	0.4587	1.6698	0.512	0.393	0.5794	0.7511	0.6619	1.171	1.5326	1.867	0.7965	1.195	1.151	1.8191	1.267	1.184	0.9729	4.5186	4.012
9030603A05	Miscellaneous	ICSBP1	Mm.249937	Hs.14453	1.4554	2.3193	0.572	1.9351	1.1385	0.8011	0.831	0.6954	1.0319	1.317	1.1693	2.324	1.791	2.136	1.0762	1.395	1.528	1.7572	2.476	1.444	1.274	0.9393	4.762
231004H42	Miscellaneous	MEF2C	Mm.24001	Hs.368950	1.0073	1.5196	0.792	0.5014	0.4258	1.2317	0.736	0.7728	0.6109	0.9083	0.7009	1.153	0.6102	0.928	0.6476	1	0.7	0.6995	0.572	2.567	1.0709	0.8572	2.22
2010013E14	Miscellaneous	FLJ38819	Mm.231635	Hs.115959	0.7993	0.7668	1.39	0.331	1.384	1.8586	0.754	0.8296	1.2952	1.2811	0.9677	1.398	0.6468	1.443	0.9023	1.248	1.117	1.2838	2.441	1.985	1.4894	0.7046	0.457
3110030A04	Miscellaneous	CED-6	Mm.133132	Hs.107056	0.5955	0.7816	0.741	0.2076	1.4448	0.9606	0.8	0.7244	1.2434	1.893	1.2375	1.362	0.5908	1.132	0.8743	1.426	1.327	1.1323	1.237	2.29	1.0819	0.0448	0.707
061007A18	Miscellaneous	SFRS5	Mm.43331	Hs.166975	2.0117	1.5993	2.141	0.5683	1.6943	1.0753	0.635	0.7171	1.9917	2.0894	2.7222	1.57	0.7939	1.001	0.9775	1.386	1.268	1.615	2.216	16.806	12.196	0.9816	1.084
0610011A23	Miscellaneous	ARHGDI1	Mm.2241	Hs.292738	1.7279	0.9489	2.037	0.3231	1.4376	1.9738	0.901	0.9421	1.4465	1.1353	1.4033	1.703	0.894	1.449	1.2614	1.554	1.071	1.2008	1.106	1.477	1.8575	1.2599	0.833
231004J15	Miscellaneous	EFNA1	Mm.15675	Hs.39973	0.9293	0.638	0.97	0.2595	1.3133	1.5032	0.753	0.8514	4.026	4.4689	3.624	1.863	1.304	1.3644	1.785	1.8157	1.278	2.781	1.6241	0.6468	0.647		
241003E11	Miscellaneous	TXNL2	Mm.267692	Hs.42644	1.2616	0.9368	1.456	0.3404	1.6435	1.2565	0.958	1.1549	0.7687	1.3804	0.9977	1.789	0.9732	1.534	0.8896	1.469	1.133	1.2728	1.234	1.594	1.5158	0.658	0.822
201007002	Miscellaneous	LENG8	Mm.22831	Hs.380446	1.0573	0.9404	1.376	0.2659	1.3178	1.1449	1.407	1.8733	1.1561	1.7686	1.2595	1.72	0.7655	1.841	0.8875	1.425	1.147	1.6937	1.051	2.3	1.2579	0.3417	0.685
181005H01	Miscellaneous	SFRS4	Mm.2478	Hs.76122	0.399	0.9139	0.324	0.6439	0.6001	0.9068	0.375	0.3882	0.4525	0.6896	0.4442	1.166	0.7588	0.827	0.4976	0.579	0.576	0.6987	0.358	7.031	8.1111	3.5512	0.726
0610041G12	Miscellaneous	DIABLO	Mm.46716	Hs.169611	0.9254	0.6862	0.28	0.6473	0.8501	1.2819	0.965	0.9566	2.6646	2.9476	2.1601	1.313	0.9597	1.013	0.9347	0.729	1.07	1.2305	0.834	1.791	1.4268	2.9798	0.591
6330408J11	Miscellaneous	CGN	Mm.87634	Hs.18376	1.625	1.5825	0.93	1.0934	1.4358	0.9281	0.868	1.1718	0.829	1.3046	0.6079	0.967	0.9762	0.848	0.6242	1.152	1.2042	1.188	1.628	1.8769	1.8444	0.435	
4921513I03	Miscellaneous	CRB1	Mm.158473	Hs.444511	1.4277	0.8819	1.024	0.7793	1.9737	1.6134	1.136	1.0025	1.7818	2.1638	1.4085	1.233	1.1816	1.282	1.4325	1.363	1.26	1.4617	0.984	1.106	1.4662	1.9726	0.447
4921514D13	Miscellaneous	DAP3	Mm.29028	Hs.270920	1.0976	1.027	0.673	0.6763	1.4353	1.2523	0.682	1.1102	1.5669	2.4657	1.3894	1.249	1.0404	1.294	1.4001	1.481	1.343	1.1797	1.152	1.505	1.6409	1.5251	0.439
130002E027	Miscellaneous	RHPN2	Mm.266600	Hs.335798	1.3681	0.9216	0.64	0.289	0.3581	0.5458	0.7653	0.7835	0.8834	1.3855	1.4011	1.1	0.841	1.214	0.6983	1.365	1.197	1.1831	1.482	3.918	2.2999	1.347	0.611
1700056A21	Miscellaneous	AVEN	Mm.292041	Hs.63168	1.8732	2.2935	0.883	2.0133	1.6714	0.8994	1.2	0.6047	1.0277	2.9054	1.0404	2.355	2.1756	1.457	1.0926	1.142	1.404	1.3296	1.563	3.092	1.5513	1.9795	0.501
5430439E07	Miscellaneous	TP73	Mm.103175	Hs.192132	1.2104	1.2264	0.685	0.7763	1.5309	1.3606	0.906	1.1114	1.7458	1.9063	0.6537	1.6	1.6349	1.195	1.8709	0.828	0.9561	0.972	1.492	1.7357	2.3729	0.704	
23100318	Miscellaneous	ASH2L	Mm.27706	Hs.6856	1.3869	1.7894	1.157	1.509	2.4762	1.254	1.133	1.1065	1.1401	3.8331	1.4998	1.738	1.6319	1.021	1.5121	0.941	1.355	1.4981	1.203	4.179	3.512	5.4255	0.386
5830472M02	Miscellaneous	C2																									